

# Trunk and leg kinematics of grounded and aerial running in bipedal macaques

Reinhard Blickhan<sup>1</sup>, Emanuel Andrada<sup>2</sup>, Eishi Hirasaki<sup>3</sup>, Naomichi Ogihara<sup>4,5</sup>

<sup>1</sup> Science of Motion, Friedrich-Schiller-University, Jena 07749, Germany; e-mail: reinhard.blickhan@uni-jena.de

<sup>2</sup> Institute of Zoology and Evolutionary Research, Jena 07743, Germany; e-mail: emanuel.andrada@uni-jena.de

<sup>3</sup> Primate Research Institute, Kyoto University, Inuyama, Aichi 484-8506, Japan; e-mail: hirasaki.eishi.6x@kyoto-u.ac.jp

<sup>4</sup> Department of Mechanical Engineering, Keio University, 3-14-1 Hiyoshi Kohoku-ku, Yokohama 223-8522, Japan; e-mail: ogihara@mech.keio.ac.jp

<sup>5</sup> Department of Biological Science, Graduate School of Science, The University of Tokyo, 7-3-1 Hongo Bunkyo-ku, Tokyo 113-0033, Japan; e-mail: ogihara@bs.s.u-tokyo.ac.jp

**Keywords:** macaque locomotion, joint angles, coordination, gait

## Summary statement

In macaques, coordination of leg and trunk segments for bipedal locomotion indicates a running gait with limited ability for energy storage.

## Abstract

Across a wide range of Froude speeds, non-human primates such as macaques prefer to use grounded and aerial running when locomoting bipedally. Both gaits are characterized by bouncing kinetics of the center of mass. On the other hand, a discontinuous change from pendular to bouncing kinetics occurs in human locomotion. To clarify the mechanism underlying these differences in bipedal gait mechanics between humans and non-human primates, we investigated the influence of gait on joint kinematics in the legs and trunk of three macaques crossing an experimental track. The coordination of movement was compared with observations available for primates. Compared to human running, macaque leg retraction cannot merely be produced by hip extension, but needs to be supported by substantial knee flexion. As a result, despite quasi-elastic whole-leg operation, the macaque's knee showed only minor rebound behavior. Ankle extension resembled that observed during human running. Unlike human running and independent of gait, torsion of the trunk represents a rather conservative feature in primates, and pelvic axial rotation added to step length. Pelvic lateral lean during grounded running by macaques (compliant leg) and human walking (stiff leg) depends on gait dynamics at the same Froude speed. The different coordination between the thorax and pelvis in the sagittal plane as compared to human runners indicates different bending modes of the spine. Morphological adaptations in non-human primates to quadrupedal locomotion may prevent human-like operation of the leg and limit exploitation of quasi-elastic leg operation despite running dynamics.

## Introduction

The kinetics of the center of mass (COM) indicates that Japanese macaques trained for bipedal locomotion use grounded and aerial running with the path of the COM reaching its deepest point during midstance, and avoid pendular walking (Ogihara et al., 2018). The axial effective leg, connecting the hip (greater trochanter) and the center of pressure, shows quasi-elastic behavior (rebound), i.e., leg shortening is followed by leg lengthening. A slight shorting of the leg at lift off during grounded running, and a slight lengthening of the leg during aerial running remain (Blickhan et al., 2018). Due to the inherent redundant nature of the three-segmented leg, different joint coordinations can lead to similar leg lengths. Segmentation and angular configurations found during human running are optimal with respect to minimum total joint torque (Seyfarth et al., 2001). This angular configuration allows the quasi-elastic operation of the leg to be translated into quasi-elastic operation of the knee and ankle joint (Günther and Blickhan, 2002; Novacheck, 1998). In the macaque leg, the ratio of relative segment lengths (thigh:shank:foot = 1:1:0.5) is not far from the human segmentation (ca. 1:1:0.4; Günther et al., 2004; Seyfarth et al., 2001), and human-like joint kinematics might be expected. During pronograd bipedal locomotion, the direction of the ground reaction force is shifted away from the hip towards the COM, enforcing deviations in joint kinematics (human, Aminiaghdam et al., 2017; bird, Andrada et al., 2014). However, the moderate trunk flexion (<30 deg; Blickhan et al., 2018) in bipedal macaques is not sufficient to induce the stark deviations in joint kinematics with respect to the human example observed. Similar to birds, macaques flex the knee throughout their stance (Ogihara et al., 2010). This was also reported for the capuchin (Demes, 2011) and for chimpanzees (Pontzer et al., 2014). In small- to medium-sized birds, the crouched leg geometry allows a rebound at the metatarsal joint (e.g., Andrada et al., 2013; Daley et al., 2007) and is optimal with respect to minimal joint work (Rode et al., 2016). The crouched posture diminishes leg stiffness (Blickhan et al., 2018), leading to the prevalence of grounded running in birds and bipedal locomotion in non-human primates.

Above trunk posture, trunk movement and deformation influence the operation of the leg. In humans and macaques, trunk kinematics differs during bipedal locomotion. In-phase axial rotation of the thorax and pelvis is observed in macaques (Ogihara et al., 2010), but rotation is out of phase in bipedal locomotion of humans and chimpanzees (Thompson et al., 2018). During the single-support phase, the pelvis rises on the swing leg side in macaques (Ogihara et al., 2010) and chimpanzees (O'Neill et al., 2015), but basically the opposite occurs in human walking. The range of yaw (lateral lean) of the pelvis is much larger for macaques and chimpanzees than for humans and enhances step length (O'Neill et al., 2015). In human locomotion, kinematics and coordination of the trunk segments depend on gait (walking: Stokes et al., 1989; running: Preece et al., 2016). Roll (axial rotation) of the pelvis enhances stride length during walking, but reduces stride length during running. Pelvic yaw lowers the hip after touch down and then slightly lifts it at midstance during walking, but the hip is lifted after touch down and then is rapidly lowered until lift off of the leg during running. Pelvic anterior tilt increases and decreases while walking, and shows the inverse behavior while running. By contrast, such discontinuous changes are currently not observed in primate locomotion.

In macaques, adaptations of the leg and trunk musculoskeletal system to quadrupedal locomotion could limit convergence to configurations with minimum joint torque (Seyfarth et al., 2001) for bipedal locomotion (Ogihara et al., 2010). In fact, despite bipedal training and regular bipedal performance, macaques still prefer quadrupedal locomotion where the leg operates at a much more flexed angle with respect to the trunk. This especially affects thigh extension with respect to the pelvis and the trunk. Understanding how such musculoskeletal constraints imposed on the trunk and leg affect the whole-body dynamics and mechanics of bipedal gait may have profound implications for understanding the evolution of human bipedal locomotion.

The present study therefore aims to investigate the trunk and leg kinematics of Japanese macaques trained for bipedal locomotion to illuminate the extent to which dynamic requirements and muscle-skeletal constraints shape the space of preferred kinematics of bipedal locomotion. With

kinematic analysis, we investigated the time course of the angles in leg joints and trunk segments in macaques during bipedal grounded and aerial running. We did not observe a single walk in our experiment. We hypothesize that joint kinematics and coordination converge for human aerial running with increasing speed. In particular, during the stance phase, we expect the leg joints to be more extended, to show a rebound behavior in the knee, and to show pelvic movement that supports a running gait. Similarities and differences compared to observations of human locomotion will be used to identify possible limitations and constraints.

## Methods

### Animals

Three regularly trained performing macaques, *Macaca fuscata* Blyth 1875, from the Suo Monkey Performance Association (Kumamoto, Japan) participated in the experiment (comp. Blickhan et al., 2018; Ogihara et al., 2018). The macaques (Ku, Po, and Fu) were all adult males (age: 15, 13, 12 years; mass: 8.64, 8.81, 8.79 kg, respectively) that had been trained for bipedal walking and performing since the age of about 1 year. The grand mean leg lengths of the effective leg ( $l_{\text{hip0}}$ ) between touch down and takeoff were 0.399, 0.339, and 0.405 m, respectively.

### Experimental setup

The macaques ran across a flat wooden track (length: 5 m). Kinematics were captured with an eight-camera infrared motion-capture system (Oqus 3+, Qualisys, Göteborg, Sweden) at a rate of 200 frames or samples per second. Details of the experimental setup and procedure are provided in Ogihara et al. (2018).

### Ethical statement

The experiments were approved by the Animal Welfare and Animal Care Committee, Primate Research Institute, Kyoto University. All institutional guidelines were followed for this study. The macaques were easily motivated to walk bipedally using a reward system. The speed of locomotion

was selected by the macaques, and the experiments were stopped when any signs of unwillingness were observed.

## Procedure

A total of 15 reflective markers were attached to the acromion, sternum xiphoid, tenth thoracic vertebra, anterior superior iliac spine, sacrum, greater trochanter, lateral epicondyle, lateral malleolus, and fifth metatarsal head of each participating animal. Static trials were used to estimate the medial joint positions (medial epicondyle, medial malleolus, and second metatarsal head; Fig. 1A-C). Extrapolation of joint centers was achieved by taking the anatomical distances of the joints from markers obtained from the static trials and computed tomography data for the greater trochanter (Ogihara et al., 2009) and extrapolating these from the outer markers in the direction perpendicular to the leg plane (see below). The local systems of coordinates (Coo) were defined by specifying  $\vec{e}_z$  and  $\vec{e}_y$ ,  $\vec{e}_x = \vec{e}_y \times \vec{e}_z$ :  $Coo_{thigh}$  with  $\vec{e}_{zthigh}$  parallel to the line connecting the knee and greater trochanter and with  $\vec{e}_{ythigh}$  being perpendicular to the leg plane defined by the greater trochanter, lateral epicondyle, and lateral malleolus;  $Coo_{shank}$  with  $\vec{e}_{zshank}$  parallel to the line connecting the ankle and the knee and with  $\vec{e}_{yshank}$  being perpendicular to the leg plane;  $Coo_{foot}$  with  $\vec{e}_{zfoot}$  directed from the medial half of the foot-width from the 5<sup>th</sup> metatarsal head to the extrapolated ankle, and with  $\vec{e}_{yfoot}$  being perpendicular to the plane defined by the foot and shank. In addition, local systems of coordinates of the thorax and pelvis were specified. The system of coordinates of the thorax (tho) was located in the centroid of the midpoint sternum xiphoid and T10, left and right acromion with  $\vec{e}_{ztho}$  pointing from the midpoint sternum xiphoid to the midpoint left and right acromion, and  $\vec{e}_{xtho}$  being perpendicular to the plane defined by center T10 and left and right acromion. The system of the pelvis (pel) was located midway between the left and right anterior superior iliac spine (ASIS) and sacrum with  $\vec{e}_{zpel}$  pointing from the sacrum to midway between the left and right ASIS, and  $\vec{e}_{xtho}$  being perpendicular to the plane defined by the sacrum and right and left ASIS. (Stick figure including coordinate systems: Fig. 2). To facilitate interpretation

and comparison with the literature, the pelvic system of coordinates was rotated by the rotation angle  $\beta_{TD}$  ( $\vec{e}_y$ ) at touch down towards the head, arms, and trunk (HAT) system.

We here describe the changes of the following angles ( $\theta$ ) between two vectors ( $-\vec{e}_1; \vec{e}_2$ ):  $\theta_{ankle}$  ( $-\vec{e}_{zfoot}; \vec{e}_{zshank}$ );  $\theta_{knee}$  ( $-\vec{e}_{zshank}; \vec{e}_{zthigh}$ );  $\theta_{hip}$  ( $-\vec{e}_{zthigh}; \vec{e}_{zhat}$ ) as well as the rotation angles ( $\alpha$  with respect to  $\vec{e}_x'$ ,  $\beta$  with respect to  $\vec{e}_y$ ,  $\gamma$  with respect to  $\vec{e}_z''$ , where ' and '' indicate the orientation of the vectors after the first and second rotation of the coordinate system) necessary to transform the distal system of coordinates into the proximal system. The Cardan rotation sequence y x'z'' was selected to first follow the component with the highest expected rotation. Due to this definition,  $\theta_{hip,knee,ank} \approx \beta_{hip,knee,ank} + 180$  deg. With respect to  $\theta, \beta_{hip}$  differences amount to  $2+(180)$  deg only, despite measuring with respect to HAT ( $\theta$ ) or the pelvis ( $\beta$ ). We documented both angles to facilitate reading and comparison with the literature. In the leg (ankle = ank, knee = kne, hip = hip), changes in  $\beta$ ,  $\alpha$ , and  $\gamma$  are termed flexion or extension, abduction or adduction, and lateral-medial rotation, respectively. Hip rotation angles were estimated as rotations between the systems of coordinates of the thigh and the pelvis. Due to the definition of the coordinate systems, knee extension  $\beta_{kne} = \theta_{kne}$  and adduction and medial rotation at the knee joint are 0. The terms flexion and extension defined by  $\theta$  and  $\beta$  are used for all joints similarly. Decreasing angles indicate flexion, and increasing angles indicate extension. The range of  $\theta_{hip,kne,ank}$  ( $\beta_{hip,ank}$ ) is from 0 deg ( $-180$  deg) for complete flexion to 180 deg (0 deg) for complete extension with the adjoining segments being aligned. According to the definitions of the International Society of Biomechanics (ISB; Wu et al., 2002), ankle flexion<sub>ISB</sub> =  $\theta_{ank} - 90$  deg =  $\beta_{ank} + 90$  deg with flexion<sub>ISB</sub>  $\geq 0$  corresponding to plantar flexion and flexion<sub>ISB</sub>  $< 0$  corresponding to dorsi flexion. For the lumbar (lum), rotations between the pelvis and the thorax  $\beta$  are termed flexion ( $\beta$  decreasing) or extension ( $\beta$  increasing),  $\alpha$  lateral flexion, and  $\gamma$  torsion.  $\beta_{lum} = 0$  deg if the thorax and pelvis are aligned.  $\beta_{lum} < 0$  deg indicates that the thorax is bent anteriorly with respect to the pelvis. For the movements of the pelvis and thorax with respect to the laboratory system of coordinates,  $\beta$ ,  $\alpha$ , and  $\gamma$  are termed pitch (forward tilt), yaw

(lateral lean), and roll (axial rotation), respectively.  $\beta_{pel,tho} = 0$  deg indicates alignment.  $\beta_{pel,tho} > 0$  deg indicates anterior pitch of the segment.

As separate averaging of the contact and the swing phase led only to minor deviations, we here documented the time courses of means  $\pm$  standard deviation (SD) of complete strides during grounded running and running, respectively. For regression, we used  $Froude\ speed = \sqrt{v^2 / l_{hip} g}$  with  $v$ : speed of the animal;  $l_{hip}$ : length of the effective leg;  $g$ : gravitational acceleration.

To describe phases of the different movements, especially for movements of the trunk segments, a harmonic function consisting of two terms, the first and second harmonics, were fit to the time course of the stride of each trial using a nonlinear fit (Fig. 1E).

$$y = a_0 + a_1 \sin(2\pi \cdot (t + \varphi_1)/100) + a_2 \sin(2 \cdot 2\pi \cdot (t + \varphi_2)/100), \quad (1)$$

where  $t$  is time [% T],  $T$  is the stride period,  $a_{0,1,2}$  are the amplitudes [deg], and  $\varphi_{1,2}$  are the phases [% T]. The phase is thus measured with respect to the touch down of the right leg. A time course similar to a sinus wave would have a phase shift of 0% T, and a cosine-like course would have a phase shift of 25% T. The second harmonics describes contributions with double frequency. The restriction to the dominant harmonics facilitates extraction of basic principles.

To describe the potential rebound period of knee and ankle angles ( $\theta$ ) and leg length (replace  $\theta$  by  $l$ ) during the stance (see Fig. 1F), three loci are used:  $\theta_{TD}$ : maximum after touch down within 10% T;  $\theta_{min}$ : local minimum after touch down;  $\theta_{LO}$ : maximum after minimum or value at lift off. Based on this, we defined the rebound amplitude referring to the range of values repeated during the stance:  $reb = \min(\theta_{TD} - \theta_{min}, \theta_{LO} - \theta_{min}) [deg]$ , the rebound gap,  $gap = \theta_{LO} - \theta_{TD} [deg]$ , and the relative rebound gap,  $rgap = gap / \max(\theta_{TD} - \theta_{min}, \theta_{LO} - \theta_{min})$ , with  $rgap = -1$  or  $+1$  for  $reb = 0$  and  $rgap = 0$  for  $\theta_{LO} = \theta_{TD}$ .

The influence of speed (covariate) and gait (factor) was investigated with a general linear model with IBM®SPSS® (Armonk, NY, USA). Custom software was written in MATLAB 14 (MathWorks, Natick, MA,

USA). Comparisons between means were done after checking for normal distributions (KS-test) either with the Wilcoxon test and dependent Student's t-test or, in the case of independent samples, with the Mann–Whitney U-test or independent Student's t-test. With respect to the phase of the harmonic analysis, circular statistics (Berens, 2009) including Rayleigh's test for significance of the means were used to calculate mean phases, SDs, and circular-linear correlations with Froude speed. Because they were based on the same set of experiments (three animals; sample size: grounded running  $n = 76$ , aerial running  $n = 20$ ), all tests were considered to be multiple tests (Bonferroni, 441 comparisons; Chen et al., 2017). The time courses of angles are available at [10.6084/m9.figshare.12029592](https://doi.org/10.6084/m9.figshare.12029592).

## Results

### Leg time courses:

The time courses of the angles were very similar between grounded running and running (Fig. 3; Table 1). The observed changes in the angles (for all joints combined including range, values at touch down and lift off, rebound) can be attributed to speed ( $p < 0.000$ ) rather than gait (n.s.; Generalized Linear Model, Bonferroni: 441).

During contact, the thigh retracted and extended with respect to the HAT ( $\theta_{hip}$ ) and pelvis ( $\beta_{hip}$ ; Fig. 3A, B). Protraction started at the end of the stance (ca. 40% T) and was completed in the early swing phase. Compared to grounded running, the movement range increased, and the thigh was more extended at lift off during aerial running (Table 1). The scatter of hip extension was high compared to the values observed for the other angles. This was due to trial-dependent postures. Hip extension approached 150 deg during aerial running but never reached 180 deg. The thigh was abducted slightly, and abduction,  $\alpha_{hip}$ , increased during the last third of the stance (Fig. 3B). During swing, the thigh was adducted. Synchronously, the thigh rotated medio-laterally ( $\gamma_{hip}$ ) and returned during swing.

The knee joint flexed ( $\theta_{kne}$ ) throughout the stance (Fig. 3A). The knee was much more flexed at lift off than at touch down both during grounded and aerial running (Table 1).  $\theta_{kne}$  at touch down decreased with speed (Fig. 4; Table 1). Gait did not affect the operation of the knee. After reaching a flexion of about 100 deg before midstance in the middle of the stance phase, the knee slightly extended, and then flexion continued until lift off. This minor oscillation of the knee angle was more pronounced during running. Flexion ended at the beginning of the swing period. After reaching maximum flexion, the knee extended until late swing, and then it flexed to prepare for touch down. The range of knee flexion exceeded the range of hip extension.

The ankle slightly flexed ( $\theta_{ank}$ ) at the beginning of the stance (Fig. 3A, C; Table 1), and then extended and started to flex quickly in advance of the swing phase. The net extension during the stance was highly significant. Flexion was maintained until the middle of the swing, when it quickly extended and flexed. The foot adducted ( $\alpha_{ank}$ ; Table 1) during stance and returned during swing. The range of adduction as well as its value at lift off decreased with speed (Table 1).

Leg phases:

The analysis including the first and second harmonics resulted in a good description (Fig. S1) with mean correlation coefficients above 0.88 (Table S1). For the hip, knee, and ankle angles, the phases of both the first ( $\varphi_1$ ) and second ( $\varphi_2$ ) harmonics significantly differed from a uniform distribution (exception:  $\varphi_2(\gamma_{ank})$ ). Except for  $\varphi_1(\theta_{ank})$  and  $\varphi_2(\theta_{hip,kne})$ , the phases did not depend on gait (Table S1). The large difference between  $\varphi_1$  of  $\theta_{hip}$  and  $\theta_{kne}$  of 52% T for grounded and 54% T for aerial running indicated the general counter-operation of these joints (extension versus flexion). The ankle joint did not simply follow the inverse of the knee joint, but  $\varphi_1$  was shifted by ca. 13% T.  $\varphi_2$  was rather similar for the three angles (difference <3% T/2). These synchronous contributions were especially visible during the swing of the leg. Within the hip, adduction and medial rotation were roughly out of phase. In contrast,  $\varphi_1$  was very similar for all components of rotation at the ankle joint. The obvious differences in the time course can be attributed to the second harmonics with high contributions by  $a_2$ , especially for  $\beta_{ank}$ .

Trunk time courses:

Lumbar extension ( $\beta_{lum}$ ; Fig. 6A) was moderate and higher during running (Table 1). After a short flexion, extension reached a plateau at mid-stance during grounded running or a maximum in the last third of the stance during running. Then the lumbar region flexed until the beginning of the stance. The range of extension increased with gait, and its value at lift off increased with speed (Fig. 7; Table 1). This effect indicated a speed-related asymmetry within the two steps of a stride. At touch down, our procedure oriented the pelvic coordinate system along the HAT axis (see methods), and  $\beta_{lum}$  was thus zero at this instant. Lateral flexion,  $\alpha_{lum}$ , and torsion,  $\gamma_{lum}$ , were much more pronounced (Table 1). With respect to the pelvis, the thorax ipsilaterally extended until almost the end of the stance (ca. 45% T) and then flexed steadily, reaching a minimum at the end of the swing (ca. 95% T). This movement was reflected by torsion. With respect to the thorax, the pelvis rotated outward until almost the end of the stance phase and then inward until the late stance. In contrast to lateral flexion, torsion was higher for running than for grounded running. The range of lateral extension depended on speed and gait (Fig. 7; Table 1). With respect to grounded running, the value of torsion in aerial running was reduced, and the outward rotation was enhanced (Fig. 7; Table 1).

The thorax (Fig. 6B) showed a short pitching (forward tilt),  $\beta_{tho}$ , after touch down and then slowly recovered; this movement was repeated in the next half stride. Its range was not affected by speed or gait (Table 1). Yaw (lateral lean),  $\alpha_{tho}$ , was away from the loaded leg until the end of the stance, and it recovered until the end of the swing. Its range diminished with speed and gait. Roll (axial rotation),  $\gamma_{tho}$ , was positive during the stance with a plateau region and negative during swing. It was not affected by speed or gait.

Like the thorax, the pelvis showed only minor pitching ( $\beta_{pel}$ , Fig. 6C); however, pitching increased when running. As in the case of the thorax (Fig. 6B) and the hip flexion (Fig. 3A, B), the large scatter was due to trial-dependent postures. Minor lumbar flexion occurred before the background of considerable thoracic and lumbar pitch of about 35 deg during grounded running and 30 deg during running. Pitch first slightly diminished during the stance and reached a maximum at

about 30% T. After a weak minimum after lift off, a second maximum was reached at about 70% T. Values at touch down and lift off depended on speed and gait (Table 1). Yaw (lateral lean),  $\alpha_{pel}$ , increased until shortly before lift off and then decreased until the end of the swing. Pelvic yaw decreased with speed and was less for running than for grounded running (Table 1). The considerable roll (axial rotation),  $\gamma_{pel}$ , largely mirrored the time course of yaw. Its range increased with speed and gait (Table 1). Both time courses of the yaw and the roll of the pelvis resembled the lateral flexion and torsion of the lumbar region. With respect to the laboratory coordinate system, the pelvis had a major contribution, but the counter-moving segments amplified the relative angular displacement. Correspondingly, to understand how the absolute angular displacements measured for the thorax segment (Fig. 6B) contributed to the relative angular displacements between the pelvis and thorax (lum; Fig. 6A), the thoracic angular displacements must be inverted.

Trunk phases:

The mean correlation of truncated Fourier fit for the trunk angles during grounded running and running was above 0.92 (Table S1; Fig. S2). The trunk pitched (tilted forward) with the double period, and except for  $\beta_{lum,GR}$ , the phases of the ground term  $\varphi_1(\beta_{lum,tho,pel})$  did not differ significantly from a uniform distribution (Table S1; Fig. 5). In contrast, the phases of the second harmonics  $\varphi_2(\alpha_{lum,tho,pel}, \gamma_{pel,tho,pel})$  did not significantly differ from uniform distribution (Fig. 5; Table S1). Differences in  $\varphi_1$  between grounded running and running were in general <5% T with the exception of  $\gamma_{hip}$  (12% T). The latter was accompanied by a strongly reduced amplitude  $a_1$ . The phase of the second harmonics for the cases of significant phase values differed <4% T between grounded running and running. Pelvic roll (axial rotation),  $\gamma_{pel}$ , followed thoracic roll,  $\gamma_{tho}$ , with a shift of 17% T and 22% T deg for grounded and aerial running, respectively. This difference in rotation induced a twist,  $\gamma_{lum}$ , with extrema at 43% T and 93% T. Significant differences with respect to gait were observed for  $\varphi_2(\beta_{lum,tho})$  (Table S1).

## Discussion

In our experiments with three individuals, the animals used a running gait. We did not observe a trial that we could classify as a walk. The comparisons of our results with data available for bipedal walking and running in primates including humans illuminate how muscle skeletal constraints resulting from adaptations to quadrupedal locomotion hamper convergence to human-like kinematics.

### Comparisons of leg kinematics

The present study demonstrated that gait kinematics changed as the speed increased in bipedal locomotion of Japanese macaques. The joint angles at touch down and lift off and the ranges of joint motions differed significantly between grounded and aerial running (Fig. 3, 4, Table 1), indicating that segment kinematics was actually altered in the transition from grounded to aerial running. However, the changes were generally minor. Discontinuous changes in the coordination and amplitudes of joint kinematics were not observed in macaques. Both gaits were essentially running as demonstrated previously (Blickhan et al., 2018), mainly due to the flexed hip and knee during the stance phase of the gait and hence the relatively compliant leg of the macaque.

By comparison, the hip and knee joints of human legs are more extended during both walking and running (Fig. 8; Novacheck, 1998), leading to a relatively stiff leg. In particular, human walkers use higher leg stiffness ( $k$ ) than runners ( $Fr = 0.67$ ;  $k_{walk} = 26.1$  kN/m;  $k_{run} = 16.5$  kN/m; Lipfert et al., 2012). The extended operation of the knee in humans is reflected in the relative rebound gap ( $rgap$ ) of this joint (Fig. 9). In macaques, the relative rebound gap of the knee is very low ( $-0.87 \pm 0.12SD$ ) as in other non-human primates (bonobo:  $-1.00$ ; chimpanzee:  $-1.00$  to  $-0.99$ ; capuchin:  $-0.97$ ; D'Août et al., 2002; Pontzer et al., 2014; Demes, 2011). The rebound tended to increase slightly as speed increased (grounded running ( $3.21 \pm 2.55SD$ ) deg, aerial running ( $5.28 \pm 3.23SD$ ) deg; Fig. 9A). In contrast, the relative rebound gap of the knee is small and positive, and the rebound is much larger in human locomotion ( $rgap$ :  $0.19$  walk;  $0.29$  run; Novacheck, 1998), indicating quasi-elastic kinematics of the knee (Fig. 9) that is not observed in macaque bipedal locomotion. Note: In

our kinematic consideration describing the rebound, we ignored the retraction period of the knee after the maximum ( $t_{TD}$ , see methods, Fig. 8). Simultaneously with this period, retraction of the hip as well as ankle extension were retarded. Unloading of the leg in the late stance facilitated extension of the long toes, compensating for flexion at hip, knee, and ankle.

Thigh adduction ( $\alpha_{hip}$ ) and rotation ( $\gamma_{hip}$ ) of the macaques also differed from those of humans. Whereas the thigh of the macaque was abducted throughout the stride (ca. 10 deg), the thigh of the human leg operates at zero abduction (Novacheck, 1998). The effect of the abduction on step length was amplified by pelvic movements (see below). However, abductive movement amplitudes are even higher in humans, and the phases of the dominating first harmonics are similar in both species. Not movement, but posture was different. The rotation angle of the hip,  $\gamma_{hip}$ , in the macaque was inward as in humans (Novacheck, 1998), but rotation amplitude in the macaque was higher, and the phase of the first harmonics indicated an advance by about 14% T, indicating that the hip movement during bipedal locomotion in macaques was more three-dimensional than during human running.

Although kinematics at the hip and knee joints is different between macaque and human running, ankle joint kinematics during macaque running strongly resembled that of human running (Fig. 8). A short dorsiflexion after touch down was followed by plantar flexion until lift off for both macaques and humans (for humans, beyond lift off). This was followed by a dorsiflexion facilitating swing and then plantarflexion to reach for the new touch down, although the latter is less prominent in the human runner. In contrast, during human walking, slight plantarflexion is initially observed after heel-contact, followed by dorsiflexion during large sections of the stance, and plantarflexion to lift off the prolonged toes. Both for the human and macaque, ankle joint kinematics indicates a large contribution to leg extension during gaits with running dynamics. Correspondingly, the phases calculated for the human runner and the macaque were rather similar (Fig. 5). Additionally, the amplitude of the rebound gap in the macaque's ankle joint was also within the range of human walking and running (Fig. 9; macaque: grounded running ( $10.06 \pm 2.84SD$ ) deg, running ( $8.26 \pm 3.90SD$ ) deg; macaque treadmill grounded running: 24.71 and 31.24 deg, Ogihara et al., 2010; human

walk: 16.28 deg, human run: 20.34 deg, Novacheck, 1998). The similar ankle kinematics between macaques and humans supports the idea that macaque bipedal locomotion is essentially running. Note: The phases in foot rotation,  $\gamma_{ank}$ , depended on variable and accidental foot placement at touch down. During fast locomotion, two animals (Fu, Po) generated a distinct peak of medial rotation (ca. 10 deg) in the second half of the stance, indicating a quick readjustment of the foot during extension.

#### Comparisons of trunk kinematics

The present study demonstrated that during bipedal locomotion, the trunk kinematics of macaques was more similar to the trunk kinematics of human running than of human walking. In both macaque grounded and aerial running, the phase of pelvic pitching (forward tilting),  $\beta_{pel}$ , was rather similar between humans (Preece et al., 2016) and macaques (ca. 60% T/2; Fig. 5E). The pitch of the thorax with respect to the pelvis led by about 61% T/2 and 69% T/2, respectively. The thoracic and pelvic segments moved almost against each other (50% T/2). In contrast, during human walking, the pitch of the thorax,  $\beta_{tho}$ , leads much less than that of the pelvis ( $Fr = 0.5$ ; Andrada, 2008: ca. 11% T/2; Stokes et al., 1989: 23% T/2). Thoracic and pelvic pitching indicate a running gait and coordination that are out of phase with respect to human walking, signaling a gait-dependent bending mode of the spine. In human walking, the pelvis and thorax pitch are closer to synchronous.

The phases of the thoracic and pelvic yaw ( $\alpha$ ; lateral lean) are also similar for both the bipedal macaque and the human runner (Fig. 5D-F; lead thorax-pelvis at  $Fr = 0.5$ : macaque ca. 52% T deg; human runner 64% T; Preece et al., 2016). The phase of the pelvic yaw in macaques was also similar to that in chimpanzee's grounded running (Fig. 5F; Thompson et al., 2018). In contrast, during human walking, the lead of the thorax yaw is less (Andrada, 2008: 32% T; Stokes et al., 1989: 25% T; Thompson et al., 2015: 40% T). Amplitudes ( $a_1$ ) are about 5 deg for both the human and the macaque. This amplitude affects hip height (macaque: ca. 5 mm, human: ca. 10 mm). In human walking, the COM is lifted at midstance. The yaw of the pelvis reduces this lift and dampens the vault over the stiff leg. During grounded running of the macaque, the compliant leg gave in, and the yaw of the pelvis supported shortening of this leg. As in the case of human running, this reduced vertical fluctuation of

the COM. On the contralateral side, the yaw supported the lift of the swing leg. In contrast, yaw lowers the hip for the swing leg for the human walker. Operating near leg extension, hip height is still sufficient to support passive swinging (McGeer, 1990). The differences in gait are reflected in differences of the pelvic yaw.

Whereas pelvic and thoracic forward tilt and lateral lean are similar in the bipedal macaque and human runner, the phases of the thoracic and pelvic roll ( $\gamma$ ; axial rotation) of the running macaque resembled human walking (Fig. 5D-F) and differed with respect to human running. Whereas pelvic roll largely shortens the step length in the human runner (Preece et al., 2016:  $\phi_1 = 71\%$  T; Schache et al., 2002), it supports stride generation in all other cases ( $\phi_1 =$  ca. 21% T) including human walking. Roll of the thorax is much more variable. At  $Fr = 0.5$ , the thorax and pelvis of macaques and chimpanzees rotate almost in synchrony with each other (this study: 2% T; Thompson et al., 2015: 97% T). This explains the impression of a rather stiff trunk in the macaque. In contrast, roll in the thorax of human walkers at  $Fr = 0.5$  leads the rotation of the pelvis (Andrada, 2008: 30% T; Bruijn et al., 2008: 35% T; Pontzer et al., 2009: 41% T; Stokes et al., 1989: 35% T; Thompson et al., 2015: 33% T). However, the amplitudes of thoracic roll in human walking indicate only minor rotations that facilitate simultaneous handling, and torsion is dominated by pelvic movement. With the marked exception of human running, the phase of lumbar torsion is rather similar across species and gaits with a maximum close to touch down (this study: 31% T; Ogiwara et al., 2010: 22% T; Thompson et al., 2018: chimpanzee 18% T, human walk 22% T). During human running at  $Fr = 1.2$ , torsion is rather different (Preece et al., 2016: 80.2% T). During human running, arms and legs compensate for momentum with respect to the vertical axis (Hinrichs, 1987), and the thorax and pelvis bear the thrust against the dynamically operating arms and legs. In addition, counter-movement may accelerate the swing of the contralateral leg and reduce the anterior loading speed of the leading leg at touch down (Schache et al., 1999). In the macaque, even the slight pronograde posture increased the trunk's moment of inertia with respect to the vertical axis, diminishing the significance of arm movements. In fact, only minor arm movements were observed.

In bipedal locomotion, the trunk provides the basis to drive the contralateral movement of the legs. In bird locomotion, the stiff pronograde trunk with its high inertia with respect to the vertical axis (Beebe, 1906) counteracts leg movement, but in bipedal primates, the stiffness of the trunk (Kubo, 2006) is organized by muscle activity, and the trunk transmits the countermovement of the arms, partly balancing the vertical momentum in combination with the inertia of the trunk segments (Gracovetsky and Iacono, 1987; Kubo et al., 2006). Moments between trunk segments may contribute to dynamics during locomotion. During human walking, the amplitude of trunk torsion increases with speed (Andrada, 2008; Kubo et al., 2006; Witte, 2002) and is correlated with an increasing trunk stiffness (Kubo, 2006). Rotation of the trunk segments in human locomotion differs with gait (Prins et al., 2019). For the macaque, pelvic roll (axial rotation) and trunk torsion contributed to step length (Fig. 5,6). Using a roll pattern inherited from quadrupedal locomotion facilitates grounded running. During aerial running, step length depends rather on the momentum generated during the stance. However, macaques that were not trained for aerial running did not alter coordination.

#### The role of physical determinants and anatomical constraints

Based on global dynamics, we classified the observed gaits of the macaques as running (Ogihara et al., 2018; Blickhan et al., 2018). The aerial phase was used to distinguish between grounded and aerial running. Numerical simulations revealed that at the Froude speed of 1.0, different initial conditions (such as the leg's angle of attack) can lead to these different gaits for similar system properties, i.e., the same leg stiffness (Andrada et al., 2020). At the transition from walking to running in human locomotion, despite different global dynamics, angular kinematics changes significantly only at the ankle joint (Segers et al., 2007). In agreement with our expectations based on the numerical simulations, our results showed significant but minor changes in kinematics at the transition from grounded to aerial running for the macaque (Table 1).

Despite the similar global running dynamics, angular coordination differs strongly between macaques and humans due to the limited hip extension in the macaque. The mean hip extension

( $\theta_{hip}$ ) was increased during aerial running compared to grounded running (Table 1). This was pronounced in the overlapping speed range (Fig. 4). At the same speed, the values indicating a reduced hip excursion tended to be grounded running. However, maximum observed hip extension at high speed did not exceed the values observed at low speed (Fig. 4), confirming an anatomical constraint. The range of movement is within a few degrees framed by the movement window identified for different individuals by passive deflection (Okada and Kimura, 1985). This constraint is a result of adaptation to pronograde quadrupedal locomotion. In turn, the reduced hip extension enforces different knee kinematics during bipedal locomotion (Ogihara et al., 2007). However, such a constraint does not preclude walking. In birds, despite the limited hip extension and a strongly flexed knee, pendular walking has been observed at low speeds with extended double support (Andrada et al., 2013; Gatesy and Biewener, 1991; Rubenson et al., 2007; Stoessel and Fischer, 2012). We expected walking at lower speeds of locomotion for the macaque. Nevertheless, with increasing speed and as a consequence of a reduced double support, maintenance of high stiffness may be expensive. Correspondingly, at intermediate speeds, grounded running is also the preferred gait in small birds (e.g., Andrada, 2013). In the macaque, the limited contact length due to the limited hip extension was increased by pelvic rotation (yaw, lateral tilt; roll, axial rotation), providing the double support necessary for grounded running. At the transition speed from grounded to aerial running, the legs are able to generate sufficient momentum to overcome the limited step length by generation of an aerial phase. With further increasing speed, the limited contact length reduced the time of force generation. Again, due to the limited hip extension, the macaque may not be able to generate the higher leg stiffness necessary for higher speed. In contrast, more time and leg length are available to produce the momentum for their spectacular jumps. Different from the human runner, pelvic roll (axial rotation) was maintained during aerial running in the macaque. This may be either a reaction to the limited momentum generated by the legs, or a sign of limited coordination due to adaption to quadrupedal locomotion. Our subjects were trained for bipedal locomotion but not for running.

## Conclusion

Based on global dynamics, all trials in our experiments with bipedal macaques were classified as running. The kinematics of the ankle supports this classification. After a rebound period, the ankle joint contributed to leg extension. In contrast, at the knee, the extent of reversible joint motion during the stance was small. During bipedal locomotion, knee kinematics in non-human primates strongly differed from observations of humans independent of gait. This seems to be caused by a limited ability of leg extension in the erect bipedal posture. The oblique posture of the thigh and the bent posture of the knee are correlated with leg compliance, facilitating grounded running (Blickhan et al., 2018). The abducted posture of the thigh induces three-dimensional rotations at the ankle joint, requiring a readjustment during extension in less trained macaques. The trunk motor supports locomotion by rotation and by lateral extension of the pelvis against the thorax. When primates switch to bipedal locomotion, the adaptation for quadrupedal locomotion does not hamper the trunk support to step generation. Similarities and differences in pelvic rotation between macaques and humans are related to i. gait (yaw, lateral lean), ii. bending modes of the spine (pitch, forward tilt), and iii. the absence of arm swing (roll, axial rotation). The latter is in turn related to trunk posture. In the macaque, anatomical limitations resulting from adaptations to quadrupedal locomotion prevent an effective exploitation of spring-like leg behavior.

## Acknowledgements:

We express our gratitude to all the staff of the Suo Monkey Performance Association for their generous collaborations in these experiments. Thanks are due to Naoki Kitagawa, Kohta Ito, Hideki Oku, Mizuki Tani from Keio University, Yokohama, Japan, and Martin Götze from Friedrich-Schiller University, Jena, Germany, for helping us during data collection. We also thank Ryoji Hayakawa, ArchiveTips, Inc., Tokyo, Japan, for support and preprocessing with Qualisys. The authors would like to thank Keio University for the guest professorship appointment to R.B. that strongly facilitated this line of research. This study was supported by a research initiation grant of the DFG to R.B. (BL 236/28-1), DFG grant to EA (AN 1286/2-1), and Grants-in-Aid for Scientific Research (#10252610, #17H01452, #20H05462) from the Japan Society of Promotion of Science and a Cooperative Research Fund of the Primate Research Institute, Kyoto University to N.O.

## Competing interests

The authors declare no competing or financial interests.

## Author contributions

Conceptualization: R.B., N.O.; Methodology: R.B., E.A., N.O.; Software: R.B.; Formal analysis: R.B.; Investigation: R.B., E.H., N.O.; Resources: E.H., N.O.; Data curation: N.O.; Writing - original draft: R.B.; Writing - review & editing: E.A., N.O.; Supervision: N.O.; Project administration: N.O.; Funding acquisition: N.O.

## Funding

This work was supported by a research initiation grant of the Deutsche Forschungsgemeinschaft to R.B. (BL 236/28-1), Grants-in-Aid for Scientific Research (#10252610, #17H01452) from the Japan Society for the Promotion of Science, a Cooperative Research Fund of the Primate Research Institute, Kyoto University to N.O., and a guest professorship to R.B. from Keio University.

## References:

- Aminiaghdam, S., Rode, C., Müller, R. and Blickhan, R.** (2017). Increasing trunk flexion transforms human leg function into that of birds despite different leg morphology. *J. Exp. Biol.* **220**, 478-486.
- Andrada, E.** (2008). A new model of the human trunk mechanics in walking. Ilmenau: Universitätsverlag Ilmenau.
- Andrada, E., Blickhan, R., Ogihara, N. and Rode, C.** (2020). Low leg compliance permits grounded running at speeds where the inverted pendulum model gets airborne. *J. Theor. Biol.* **494**.
- Andrada, E., Nyakatura, J. A., Bergmann, F. and Blickhan, R.** (2013). Adjustments of global and local hindlimb properties during terrestrial locomotion of the common quail (*Coturnix coturnix*). *J. Exp. Biol.* **216**, 3906-3916.
- Andrada, E., Rode, C., Sutedja, Y., Nyakatura, J. A. and Blickhan, R.** (2014). Trunk orientation causes asymmetries in leg function in small bird terrestrial locomotion. *Proc. Roy. Soc. B.* **281**.
- Beebe, C. W.** (1906) The Bird: Its Form and Function (1906) Henry Holt and Company, New York.
- Berens, P.** (2009). CircStat: A Matlab Toolbox for Circular Statistics. *J. Stat. Softw.* **31**, 1-21.
- Blickhan, R., Andrada, E., Hirasaki, E. and Ogihara, N.** (2018). Global dynamics of bipedal macaques during grounded and aerial running. *J. Exp. Biol.* **221**, jeb178897.
- Bruijn, S. M., Meijer, O. G., van Dieën, J. H., Kingma, I. and Lamoth, C. J. C.** (2008). Coordination of leg swing, thorax rotations, and pelvis rotations during gait: The organisation of total body angular momentum. *Gait & Posture* **27**, 455-462.
- Chen, S.-Y., Feng, Z. and Yi, X.** (2017). A general introduction to adjustment for multiple comparisons. *J. Thorac. Dis.* **9**, 1725-1729.
- D'Août, K., Aerts, P., De Clercq, D., De Meester, K. and Van Elsacker, L.** (2002). Segment and joint angles of hind limb during bipedal and quadrupedal walking of the bonobo (*Pan paniscus*). *Am. J. Phys. Anthropol.* **119**, 37-51.
- Daley, M. A., Felix, G. and Biewener, A. A.** (2007). Running stability is enhanced by a proximo-distal gradient in joint neuromechanical control. *J. Exp. Biol.* **210**, 383-394.
- Demes, B.** (2011). Three-dimensional kinematics of capuchin monkey bipedalism. *Am. J. Phys. Anthropol.* **145**, 147-155.
- Gatesy, S. M. and Biewener, A. A.** (1991). Bipedal locomotion: effects of speed, size and limb posture in birds and humans. *J. Zool.* **224**, 127-147.
- Gracovetsky, S.A. and Iacono, S.** (1987) Energy transfers in the spinal engine. *J. Biomed. Eng.* **9**, 99-114.
- Günther, M. and Blickhan, R.** (2002). Joint stiffness of the ankle and the knee in running. *J. Biomech.* **35**, 1459-1474.
- Günther, M., Keppeler, V., Seyfarth, A. and Blickhan, R.** (2004). Human leg design: optimal axial alignment under constraints. *J. Math. Biol.* **48**, 623-646.
- Hinrichs, R. N.** (1987). Upper extremity function in running. II: Angular momentum considerations. *J. Appl. Biomech.* **3**, 242-263.
- Kubo, M., Holt, K. G., Saltzman, E. and Wagenaar, R. C.** (2006). Changes in axial stiffness of the trunk as a function of walking speed. *J. Biomech.* **39**, 750-757.
- Lipfert, S. W., Günther, M., Renjewski, D., Grimmer, S. and Seyfarth, A.** (2012). A model-experiment comparison of system dynamics for human walking and running. *J. Theor. Biol.* **292**, 11-17.
- McGeer, T.** (1990). Passive Dynamic Walking. *Int. J. Rob. Res.* **9**, 62-82.
- Novacheck, T. F.** (1998). The biomechanics of running. *Gait & Posture* **7**, 77-95.
- Ogihara, N., Hirasaki, E., Andrada, E. and Blickhan, R.** (2018). Bipedal gait versatility in the Japanese macaque (*Macaca fuscata*). *J. Hum. Evol.* **125**, 2-14.
- Ogihara, N., Hirasaki, E., Kumakura, H. and Nakatsukasa, M.** (2007). Ground-reaction-force profiles of bipedal walking in bipedally trained Japanese monkeys. *J. Hum. Evol.* **53**, 302-308.

- Ogihara, N., Makishima, H., Aoi, S., Sugimoto, Y., Tsuchiya, K. and Nakatsukasa, M.** (2009). Development of an anatomically based whole-body musculoskeletal model of the Japanese macaque (*Macaca fuscata*). *Am. J. Phys. Anthropol.* **139**, 323-338.
- Ogihara, N., Makishima, H. and Nakatsukasa, M.** (2010). Three-dimensional musculoskeletal kinematics during bipedal locomotion in the Japanese macaque, reconstructed based on an anatomical model-matching method. *J. Hum. Evol.* **58**, 252-261.
- Okada, M., Kimura, T.** (1985) Range of passive flexion and extension of hindlimb joints in the Japanese macaque. *J. Anthropol. Soc. Nippon* **93**, 327-335.
- O'Neill, M. C., Lee, L.-F., Demes, B., Thompson, N. E., Larson, S. G., Stern Jr, J. T., Umberger, B. R.** (2015) Three-dimensional kinematics of the pelvis and hindlimbs in chimpanzee (*Pan troglodytes*) and human bipedal walking. *J. Hum. Evol.* **86**, 32-42
- Pontzer, H., Holloway, J. H., Raichlen, D. A. and Lieberman, D. E.** (2009). Control and function of arm swing in human walking and running. *J. Exp. Biol.* **212**, 523-534.
- Pontzer, H., Raichlen, D. A. and Rodman, P. S.** (2014). Bipedal and quadrupedal locomotion in chimpanzees. *J. Hum. Evol.* **66**, 64-82.
- Preece, S. J., Mason, D. and Bramah, C.** (2016). The coordinated movement of the spine and pelvis during running. *Hum. Movement Sci.* **45**, 110-118.
- Prins, M. R., Bruijn, S. M., Meijer, O. G., van der Wurff, P. and van Dieën, J. H.** (2019). Axial thorax-pelvis coordination during gait is not predictive of apparent trunk stiffness. *Sci. Rep.-UK.* **9**, 1066.
- Rode, C., Sutedja, Y., Kilbourne, B. M., Blickhan, R. and Andrada, E.** (2016). Minimizing the cost of locomotion with inclined trunk predicts crouched leg kinematics of small birds at realistic levels of elastic recoil. *J. Exp. Biol.* **219**, 485-490.
- Rubenson, J., Lloyd, D. G., Besier, T. F., Heliams, D. B. and Fournier, P. A.** (2007). Running in ostriches (*Struthio camelus*): three-dimensional joint axes alignment and joint kinematics. *J. Exp. Biol.* **210**, 2548-2562.
- Schache, A. G., Bennell, K. L., Blanch, P. D. and Wrigley, T. V.** (1999). The coordinated movement of the lumbo–pelvic–hip complex during running: a literature review. *Gait & Posture* **10**, 30-47.
- Schache, A. G., Blanch, P., Rath, D., Wrigley, T. and Bennell, K.** (2002). Three-dimensional angular kinematics of the lumbar spine and pelvis during running. *Hum. Movement Sci.* **21**, 273-293.
- Segers, V., Lenoir, M., Aerts, P. and De Clercq, D.** (2007). Kinematics of the transition between walking and running when gradually changing speed. *Gait & Posture* **26**, 349-361.
- Seyfarth, A., Günther, M. and Blickhan, R.** (2001). Stable operation of an elastic three-segment leg. *Biol. Cybern.* **84**, 365-382.
- Stoessel, A. and Fischer, M. S.** (2012). Comparative intralimb coordination in avian bipedal locomotion. *J. Exp. Biol.* **215**, 4055-4069.
- Stokes, V. P., Andersson, C. and Forssberg, H.** (1989). Rotational and translational movement features of the pelvis and thorax during adult human locomotion. *J. Biomech.* **22**, 43-50.
- Thompson, N. E., Demes, B., O'Neill, M. C., Holowka, N. B. and Larson, S. G.** (2015). Surprising trunk rotational capabilities in chimpanzees and implications for bipedal walking proficiency in early hominins. *Nat. Com.* **6**, 8416.
- Thompson, N. E., O'Neill, M. C., Holowka, N. B. and Demes, B.** (2018). Step width and frontal plane trunk motion in bipedal chimpanzee and human walking. *J. Hum. Evol.* **125**, 27-37.
- Witte, H.** (2002). Hints for the construction of anthropomorphic robots based on the functional morphology of human walking. *J. Rob. Soc. JPN.* **20**, 247-254.
- Wu, G., Siegler, S., Allard, P., Kirtley, C., Leardini, A., Rosenbaum, D., Whittle, M., D'Lima, D. D., Cristofolini, L., Witte, H. et al.** (2002). ISB recommendation on definitions of joint coordinate system of various joints for the reporting of human joint motion—part I: ankle, hip, and spine. *J. Biomech.* **35**, 543-548.



## Figures

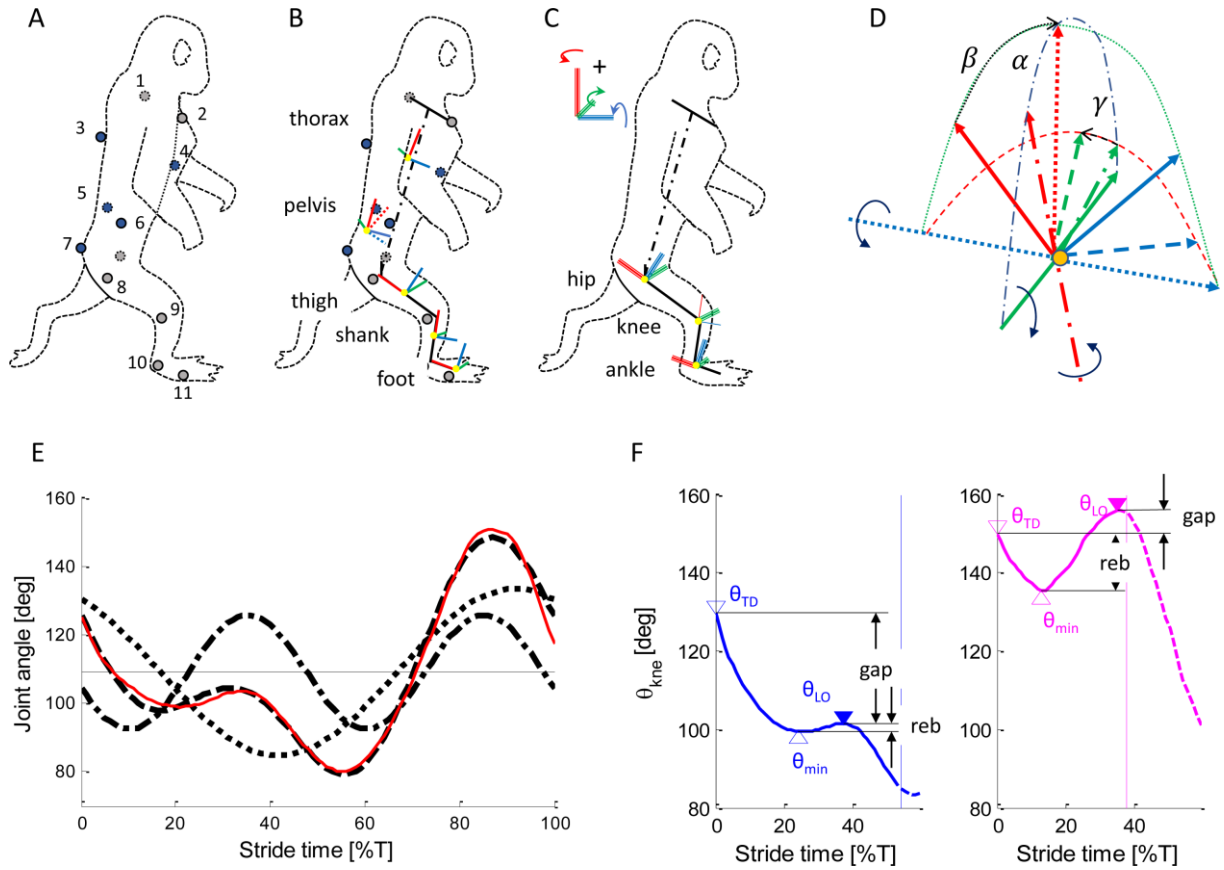


Fig. 1: Methods - Location of markers and coordinate systems (A-D), harmonic decomposition (E), and rebound (F). A) Location of markers: (1,2) left and right acromion; (3) T10; (4) sternum xiphoid; (5,6) left and right ASIS; (7) sacrum; (8) greater trochanter; (9) lateral epicondyle; (10) lateral malleolus; (11) 5<sup>th</sup> metatarsal head. Markers on the contralateral leg (lateral epicondyle, lateral malleolus, 5<sup>th</sup> metatarsal head) and the corresponding systems of coordinates of the thigh shank and foot are not depicted for clarity. B) Segments and their respective systems of coordinates. Segments: HAT (dash-dotted black line), thorax, pelvis, thigh, shank, foot (solid black lines). Coordinate systems: yellow: origin; blue:  $\vec{e}_x$ ; green:  $\vec{e}_y$ ; red:  $\vec{e}_z$ . Pelvis: dashed initial system using the markers, solid: system after touch down with  $\vec{e}_z$  parallel to HAT. C) Joint rotational axes (multiple lines). Knee:  $\vec{e}_y$  (hinge joint). Only rotations are described. D) Rotation sequence. The distal system (solid arrows) is

rotated to the proximal system (dashed arrows) by the first rotation (, dotted) around  $\vec{e}_y (\beta)$ , the second (', dash dotted) around the new  $\vec{e}_x' (\alpha)$ , and finally ("; dashed) around the new  $\vec{e}_z'' (\gamma)$ . E) Harmonic analysis of knee angle ( $\theta_{kne}$ ). Red line: original data. Black lines - dashed: harmonic decomposition  $\theta_{kne} = 109 + 24 \cdot \sin(2\pi \cdot (t + 33)) + 17 \cdot \sin(2 \cdot 2\pi \cdot (t + 55))$  deg; dotted: first harmonic:  $(109 + 24 \cdot \sin(2\pi \cdot (t + 33)))$  [deg]; dash-dotted:  $(109 + 17 \cdot \sin(2 \cdot 2\pi \cdot (t + 55)))$  deg; horizontal line:  $a_0 = 109$  deg. F) Rebound (reb) and rebound gap (gap) for the example of the macaque (left, grounded running) and the human (right, running) knee angle.  $\theta_{TD}$ : maximum after touch down;  $\theta_{min}$ : local minimum;  $\theta_{LO}$ : local maximum before lift off (end of contact: vertical line).

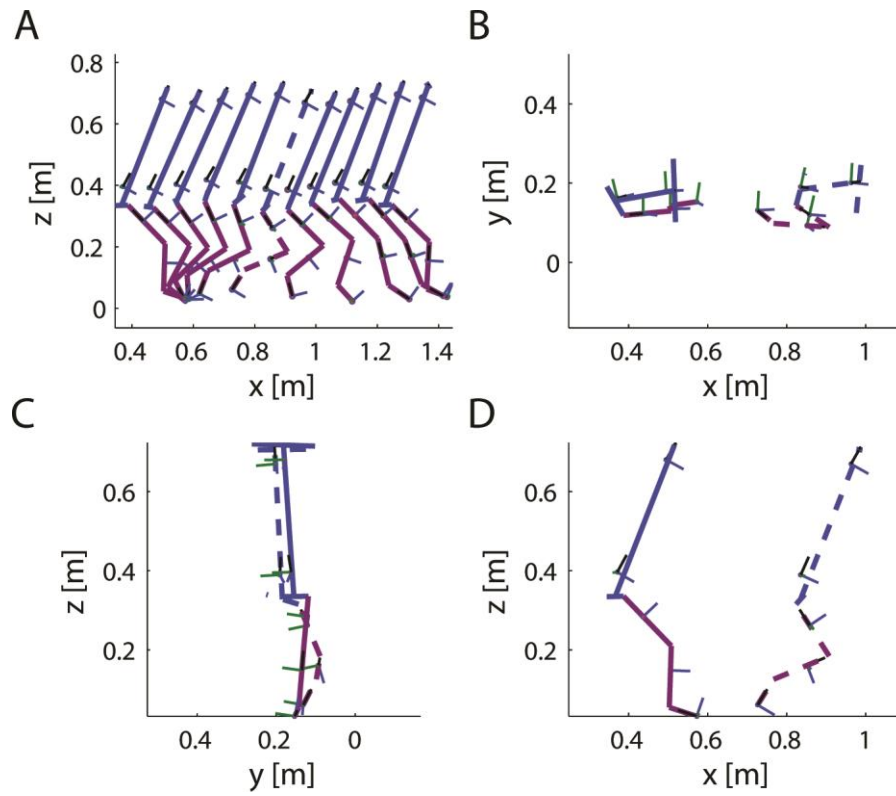


Fig. 2: Stick figures and segment fixed systems of coordinates during grounded running of a macaque (Ku). A) Sagittal projection of a complete stride. B, C, D) Transverse (B), frontal (C), and sagittal projections of the stick figures at touch down (continuous lines) and lift off (dashed lines). Extrema of rotation angles occur close to touch down and take off. Blue: HAT, magenta: right leg. Systems of coordinates from above to below: thorax, pelvis, thigh, shank, foot. Froude speed: 0.80. Duty factor: 0.53.

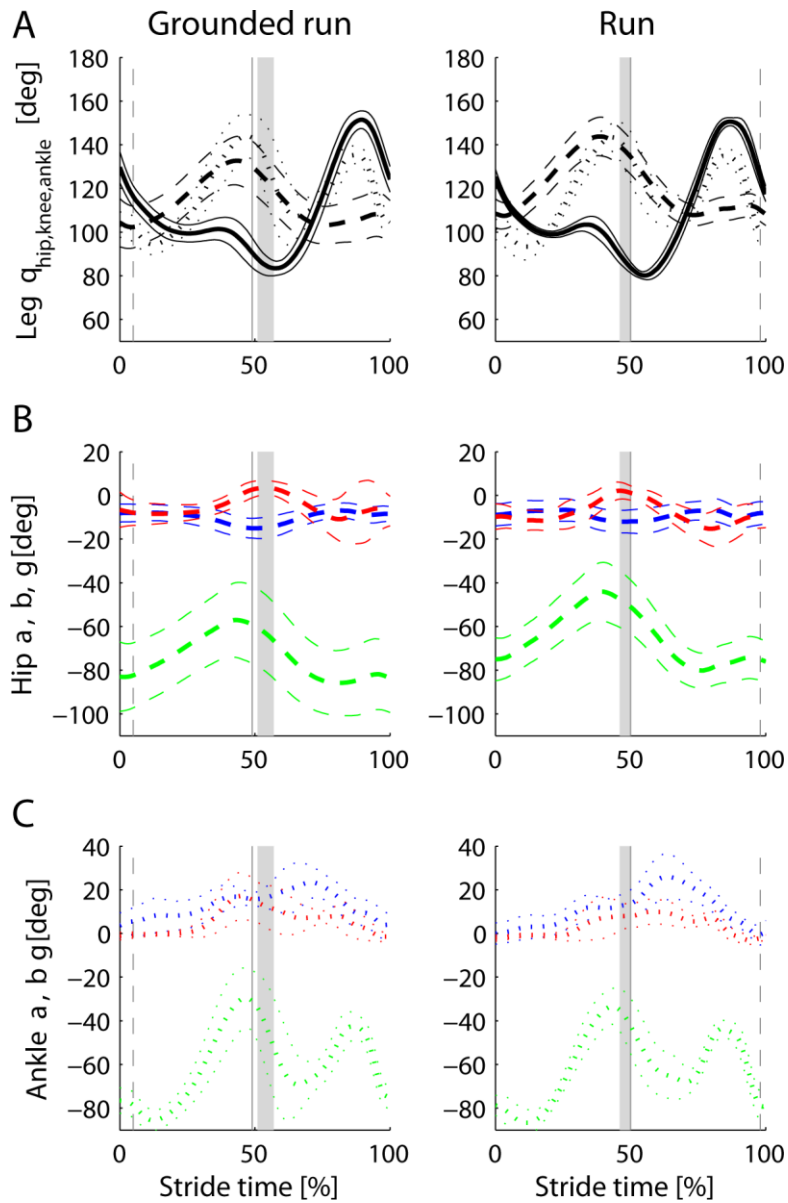


Fig. 3: Time course of mean angles (bold)  $\pm$ SD (thin lines) in the leg for grounded running and running. A) Enclosed angles  $\theta$  of the hip (dashed), the knee (solid), and the ankle (dotted). B) Hip. Rotation of the thigh with respect to the pelvis. C) Ankle. Rotation of the foot with respect to the thigh. Rotation angles. blue – adduction -  $\alpha$ ; green – extension -  $\beta$ ; red – medial rotation -  $\gamma$ . Shaded - stance swing transition  $\pm$ SD. Vertical grey line: contralateral touch down. Vertical dashed line: contralateral lift off. ISB definitions (Wu et al., 2002): ankle flexion<sub>ISB</sub> =  $\theta_{ank} - 90$  deg =  $\beta_{ank} + 90$  deg. flexion<sub>ISB</sub>  $\geq 0$ : plantar flexion. flexion<sub>ISB</sub>  $< 0$ : dorsi flexion.

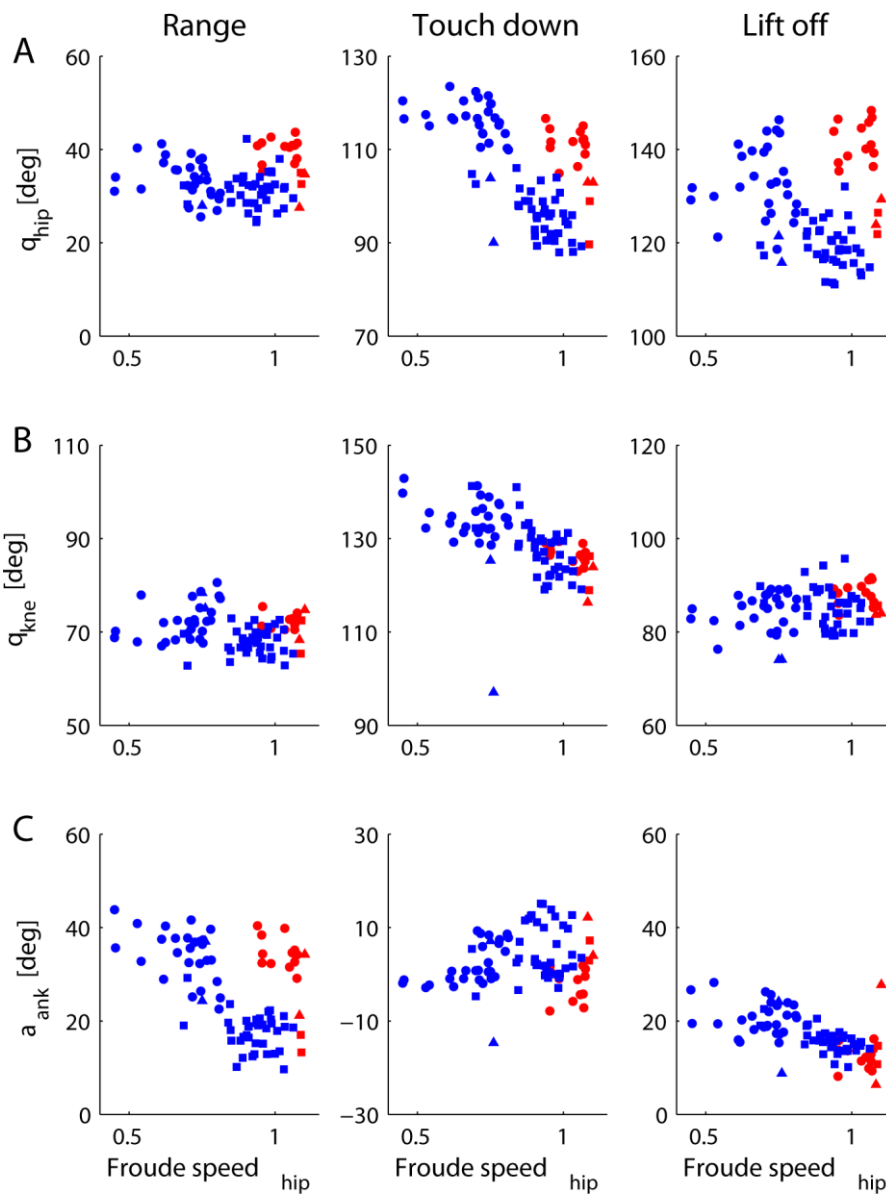


Fig. 4: Range, touch down and lift off values for hip angle  $\theta_{hip}$  (A), knee angle  $\theta_{kne}$  (B), and ankle angle  $\alpha_{ank}$  (C) with respect to Froude speed. The time course of the outlier indicating a touch down with strongly bent legs (Po; Froude speed = 0.76) resembles the other observations. Blue: grounded running; red: running; Ku: circles; Fu: squares; Po: triangles. ISB definitions (Wu et al., 2002): ankle flexion<sub>ISB</sub> =  $\theta_{ank} - 90 \text{ deg} = \beta_{ank} + 90 \text{ deg}$ ; flexion<sub>ISB</sub>  $\geq 0$ : plantar flexion; flexion<sub>ISB</sub>  $< 0$ : dorsi flexion.

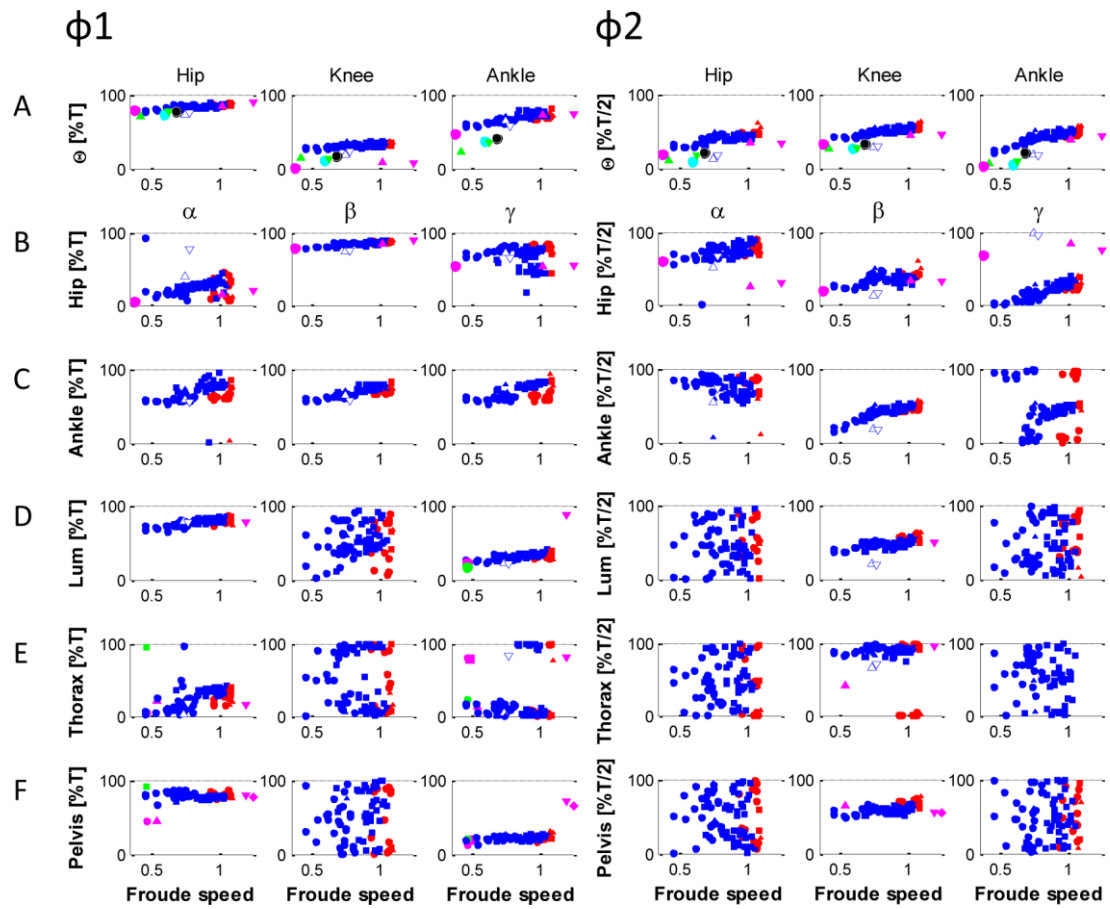


Fig. 5: Phases from 0% T to 100% T of the 1<sup>st</sup> harmonics  $\phi_1$  (column 1 to 3) and from 0% T/2 to 100% T/2 of the 2<sup>nd</sup> harmonics  $\phi_2$  (column 4 to 6) of the truncated Fourier series dependent on Froude speed. A)  $\theta$  for hip, knee, and ankle. B–F) for hip, ankle, thorax, and pelvis  $\phi_{1,2}$  of rotation components  $\alpha, \beta, \gamma$ . Lum: relative rotation between pelvis and thorax. Blue: grounded running; red: aerial running; Ku: circles; Fu: squares; Po: triangles. Estimates from literature: empty blue triangles - macaque (Ogihara et al, 2010); cyan circles – bonobo (D'Août et al., 2002); green circles, squares, triangles - chimpanzee (Thompson et al., 2015; Thompson et al., 2018; Pontzer et al., 2014); black circles – capuchin monkey (Demes, 2011). In A–C: magenta circles, upward-pointing triangles, downward-pointing triangles – human walk, run, and sprint, respectively (Novacheck, 1998). In D–F  $\alpha, \gamma$ : magenta squares, downward-pointing triangles (run), diamonds (run), upward-pointing triangles, circles - human (Bruijn et al., 2008; Preece et al., 2016; Schache et al., 2002; Stokes et al., 1989; Thompson et al., 2015; Thompson et al., 2018). Dashed horizontal line:  $\phi_1$  - 100% T;  $\phi_2$  - 100% T/2.

Insignificant differences of literature values compared to the median of the macaque (angle, species, speed):  $\varphi_1 - \theta_{hip}$ , human run, 1.02;  $\alpha_{hip}$ , human run, 1.25;  $\alpha_{pel}$ , human run, 1.20;  $\alpha_{lum}$ , macaque, 0.74, 0.77, human run, 1.20;  $\beta_{hip}$ , human run, 1.02;  $\gamma_{hip}$ , macaque, 0.75;  $\gamma_{tho}$ , macaque, 0.74;  $\gamma_{pel}$ , chimpanzee, 0.47;  $\varphi_2 - \theta_{ank}$ , human sprint, 1.25;  $\beta_{hip}$ , human run, 1.02;  $\beta_{lum}$ , human run, 1.20.

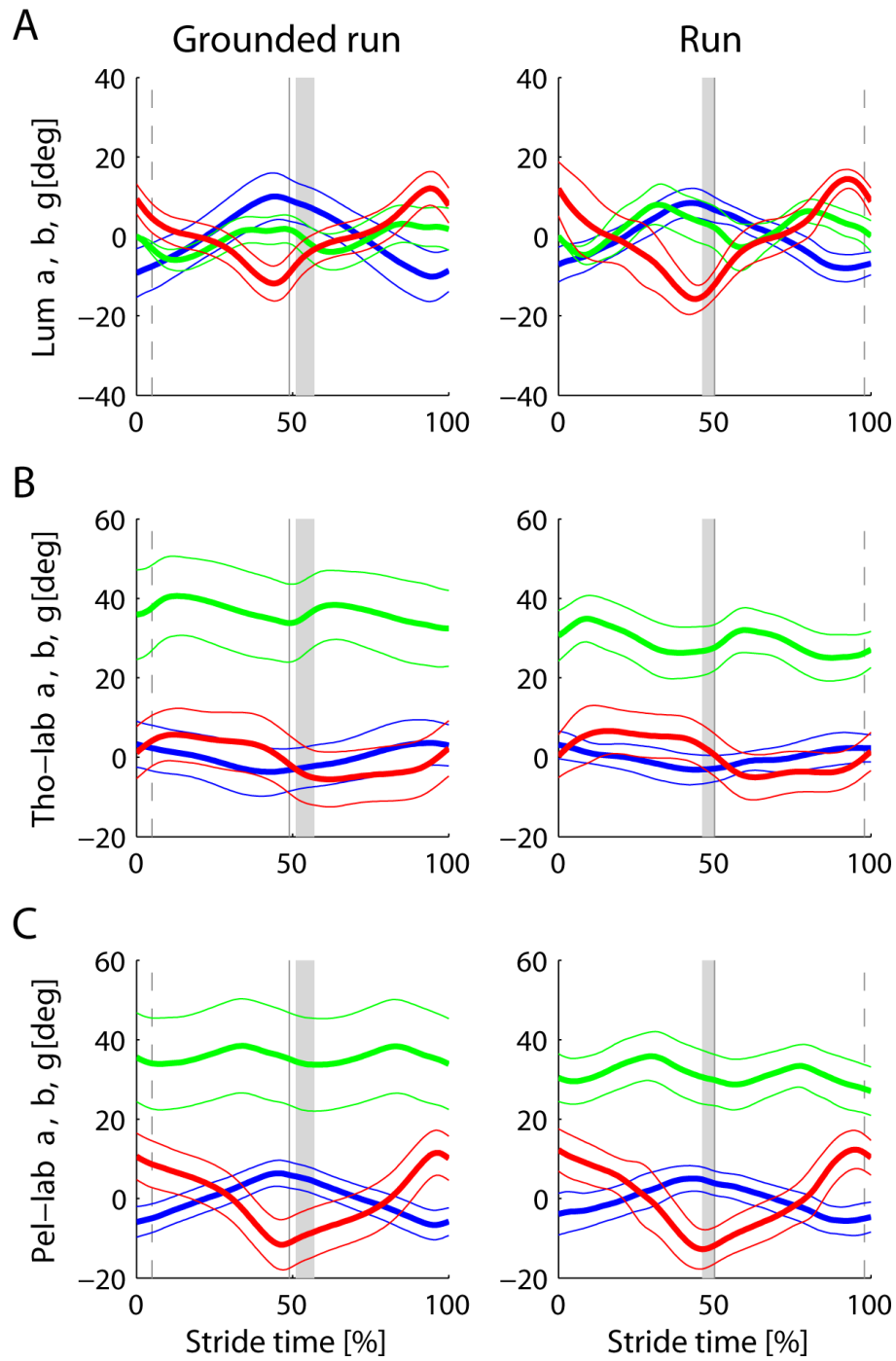


Fig. 6: Time course of mean angles (bold)  $\pm$ SD (thin lines) in the trunk of the macaque during grounded running and running. A) Rotation of the pelvis with respect to the thorax. B) Rotation of the thorax with respect to laboratory coordinates. C) Rotation of the pelvis with respect to laboratory coordinates. Rotation angles (as in Fig. 2): A) blue – lateral flexion -  $\alpha$ ; green – extension -  $\beta$ ; red – torsion -  $\gamma$ ; B, C) blue: yaw (lateral lean) -  $\alpha$ ; green – pitch (forward tilt) -  $\beta$ ; red – roll (axial rotation)

$\gamma$ . Shaded stance swing transition  $\pm$ SD. Vertical grey line: contralateral touch down. Vertical dashed line: contralateral lift off.  $\beta_{lum}$  decreasing: flexion;  $\beta_{lum}$  increasing: extension;  $\beta_{lum} = 0$  deg: thorax and pelvis aligned;  $\beta_{lum} < 0$  deg: thorax bent anteriorly with respect to the pelvis;  $\beta_{pel,tho} = 0$  deg alignment;  $\beta_{pel,tho} > 0$  deg anterior pitch of the segment.

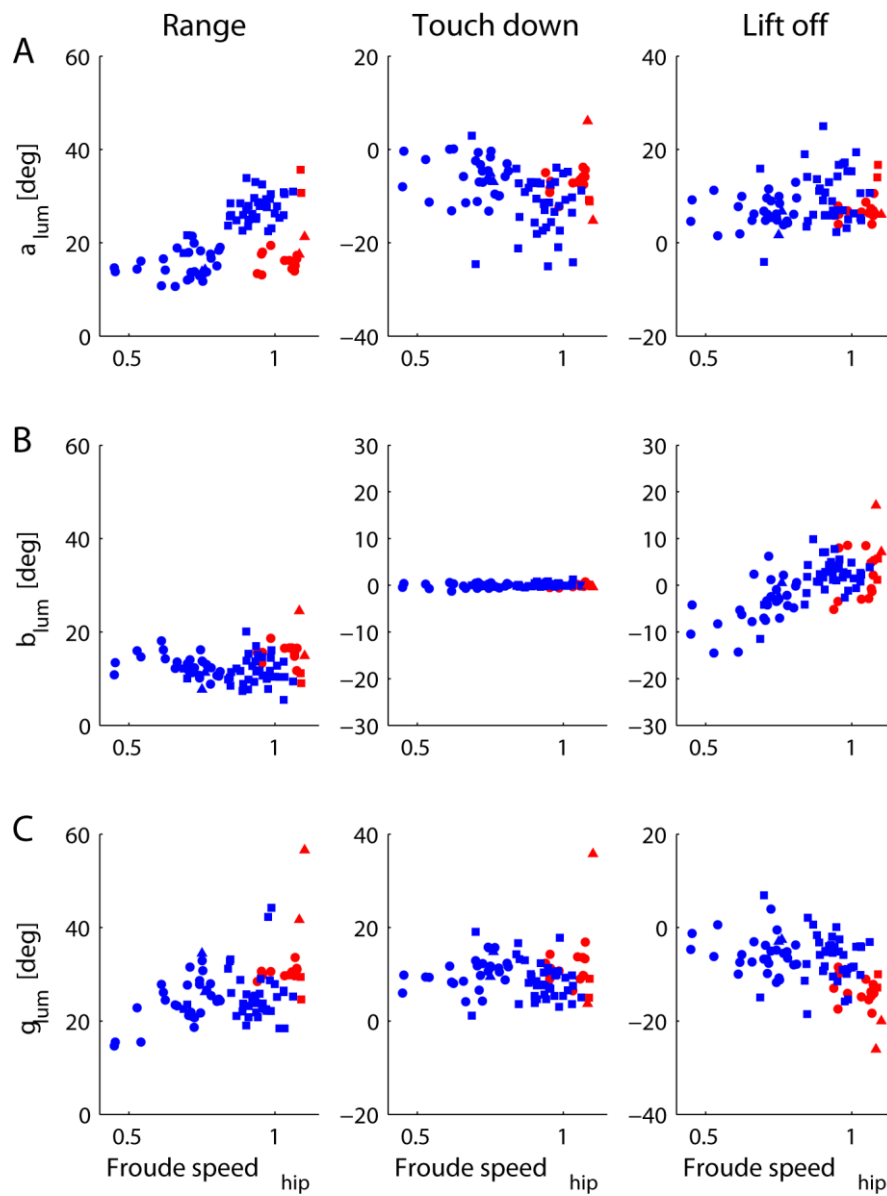


Fig. 7: Range, touch down, and lift off values for  $\alpha_{lum}$  (A),  $\beta_{lum}$  (B), and  $\gamma_{lum}$  (C) dependent on Froude speed. The low scatter of the touch down value of  $\beta_{lum}$  (B) is due to the specification of the coordinate system. Blue: grounded running; red: running; Ku: circles; Fu: squares; Po: triangles.  $\beta_{lum}$  decreasing: flexion;  $\beta_{lum}$  increasing: extension;  $\beta_{lum} = 0$  deg: thorax and pelvis aligned;  $\beta_{lum} < 0$  deg: thorax bent anteriorly with respect to the pelvis.  $\beta_{pel,tho} = 0$  deg alignment;  $\beta_{pel,tho} > 0$  deg anterior pitch of the segment.

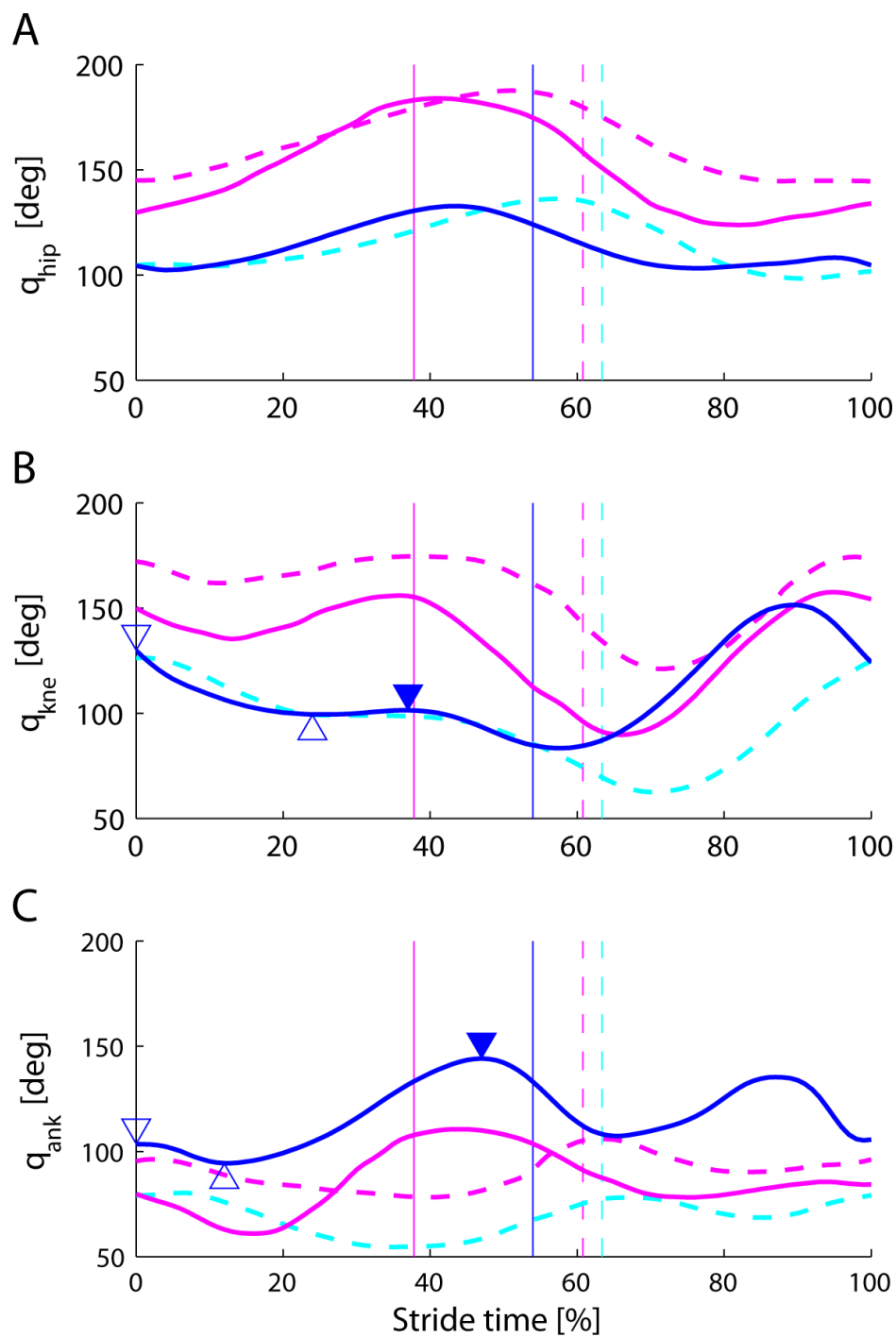


Fig. 8: Time course of the leg angles  $\theta_{hip,kne,ank}$  for the macaque (grounded running, blue solid line), the bonobo (cyan dashed line), and the human (walking, magenta dashed line; running, magenta solid line). Solid lines: running-like ankle extension; dashed lines: walking-like ankle kinematics. Vertical lines: lift off. Sources: macaque - this investigation, Froude speed: 0.82 (compare to Fig. 3A); bonobo – Daout et al., 2002, Fig. 4, mean Froude speed: 0.60; human – Novacheck, 1998, Fig. 5

(Froude speeds walk and run: 0.38 and 1.02, respectively). Triangles: open downward triangles: Maximum within 10% T after touch down,  $(t_{TD}, \theta_{TD})$ ; open upward triangles: first minimum after touch down,  $(t_{min}, \theta_{min})$ ; filled downward triangles: maximum between minimum and lift off,  $(t_{LO}, \theta_{LO})$ . ISB definitions (Wu et al., 2002): ankle flexion<sub>ISB</sub> =  $\theta_{ank} - 90 \text{ deg} = \beta_{ank} + 90 \text{ deg}$ ; flexion<sub>ISB</sub>  $\geq 0$ : plantar flexion; flexion<sub>ISB</sub>  $< 0$ : dorsi flexion.

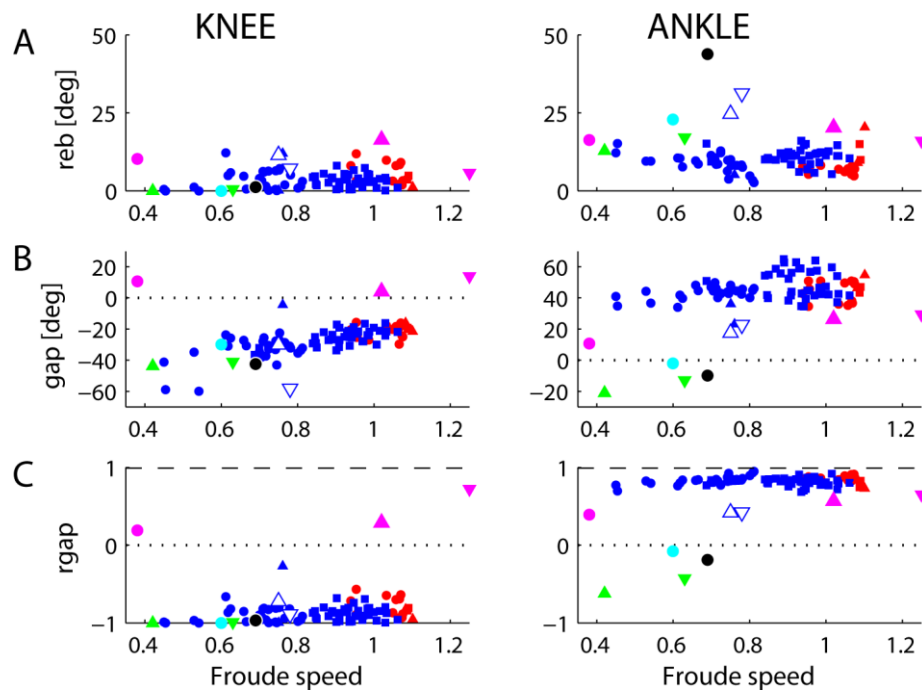


Fig. 9: Rebound amplitude (reb, A), rebound gap (gap, B), and relative rebound gap (rgap, C) for the knee (left) and ankle (right). Significance of dependence on Froude speed and gait (GLM):  $\text{reb}_{\text{kne}}$ : n.s., n.s.;  $\text{reb}_{\text{ank}}$ : n.s., n.s.;  $\text{gap}_{\text{kne}}$ : 0.000, n.s.;  $\text{gab}_{\text{ank}}$ : n.s., n.s.;  $\text{rgap}_{\text{kne}}$ : n.s., n.s.;  $\text{rgap}_{\text{ank}}$ : n.s., n.s.

Bonferroni: 441 comparisons. Estimates from the literature: empty blue triangles - macaque (Ogihara et al, 2010); cyan circles – bonobo (D'Août et al., 2002); green triangles – chimpanzee (Pontzer et al., 2014); black circles – capuchin monkey (Demes, 2011); magenta circles, upper triangles, lower triangles – human walk, run, and sprint, respectively (Novacheck, 1998). See Fig. 5. A-C.

Table 1: Range during a stride, and values at touch down and lift off of angles in degrees (comp. Figs. 3, 7) during grounded running (GR) and running (R). Significance between subjects, effects for GLM with v as a covariate ( $p_v$ ) and gait (grounded running, running;  $p_{GR,R}$ ) as a factor, and the difference between touch down and lift off ( $p_{td,lo}$ ). Bonferroni for all probabilities ( $f = 441$ ).

Angles [deg]	Gait	Range mean	SD	n $p_{GR,R}$	Touch down mean	SD	n $p_{GR,R}$	Lift off mean	SD	n $p_{GR,R}$	$P_{td,lo}$
$\theta_{hip}$	GR	32.2	4.0	n.s.	104.3	11.1	0.000	124.8	9.1	0.000	0.000
	R	38.2	4.2	0.000	108.5	6.9	0.000	138.0	8.3	0.000	0.000
$\theta_{kne}$	GR	69.9	4.0	n.s.	129.7	7.2	0.000	84.8	4.3	n.s.	0.000
	R	71.5	2.5	n.s.	125.3	3.5	n.s.	87.5	2.7	n.s.	0.000
$\theta_{ank}$	GR	58.0	7.7	0.006	103.4	5.9	n.s.	141.3	9.9	n.s.	0.000
	R	53.0	8.6	0.003	101.2	4.6	n.s.	140.6	7.9	n.s.	0.000
$\alpha_{hip}$	GR	9.6	4.2	0.017	-8.1	4.1	n.s.	-15.0	4.8	0.000	0.000
	R	7.9	3.4	n.s.	-8.9	5.3	n.s.	-12.0	5.4	0.001	n.s.
$\beta_{hip}$	GR	30.4	4.5	n.s.	-83.0	16.0	0.000	-62.6	15.6	0.000	0.000
	R	37.2	7.2	0.001	-75.0	10.1	0.000	-48.5	13.2	0.000	0.000
$\gamma_{hip}$	GR	20.4	9.5	0.044	-6.6	8.1	0.000	3.9	3.4	n.s.	0.000
	R	20.4	4.2	n.s.	-9.7	6.0	0.000	2.1	4.2	n.s.	0.000
$\alpha_{ank}$	GR	24.8	9.5	0.000	3.7	5.7	n.s.	17.8	4.0	0.000	0.000
	R	31.5	7.5	0.000	0.0	5.1	0.025	13.2	4.7	n.s.	0.000
$\beta_{ank}$	GR	67.4	9.5	n.s.	-76.5	5.9	n.s.	-32.1	13.0	n.s.	0.000
	R	56.9	11.0	0.001	-78.7	4.7	n.s.	-36.2	8.9	n.s.	0.000
$\gamma_{ank}$	GR	28.5	6.7	n.s.	-1.2	1.7	n.s.	16.5	8.3	0.001	0.000
	R	19.4	5.2	0.034	-2.0	1.5	n.s.	8.1	5.8	n.s.	0.000
$\alpha_{lum}$	GR	21.9	6.7	0.000	-9.2	6.2	n.s.	8.5	5.1	n.s.	0.000
	R	18.4	6.0	0.000	-7.1	4.5	n.s.	7.6	3.3	n.s.	0.000
$\beta_{lum}$	GR	12.1	2.7	n.s.	0.0	0.4	n.s.	-0.6	5.1	0.000	n.s.
	R	15.4	3.3	0.004	0.0	0.3	n.s.	3.3	5.8	n.s.	n.s.
$\gamma_{lum}$	GR	25.1	5.3	n.s.	9.4	3.8	n.s.	-6.1	4.5	n.s.	0.000
	R	32.2	7.1	n.s.	12.0	7.0	n.s.	-14.5	4.3	0.006	0.000
$\alpha_{tho}$	GR	9.8	3.9	0.000	3.3	5.8	n.s.	-3.1	5.4	n.s.	0.000
	R	7.6	4.1	0.000	3.1	3.6	n.s.	-3.0	3.6	n.s.	0.000
$\beta_{tho}$	GR	10.0	2.7	n.s.	35.9	11.3	0.000	35.3	8.6	0.000	n.s.
	R	11.1	2.1	n.s.	30.5	6.5	0.000	26.8	6.3	0.000	n.s.
$\gamma_{tho}$	GR	14.2	3.6	n.s.	1.2	6.6	n.s.	-3.5	7.6	n.s.	0.000
	R	15.8	5.6	n.s.	0.3	5.6	n.s.	2.1	5.8	n.s.	n.s.
$\alpha_{pel}$	GR	13.9	3.9	0.000	-5.9	3.9	n.s.	5.3	3.2	n.s.	0.000
	R	11.5	2.5	0.000	-3.9	5.4	n.s.	4.6	3.2	n.s.	0.000
$\beta_{pel}$	GR	7.0	1.5	n.s.	35.6	11.3	0.000	34.2	11.9	0.000	0.000
	R	10.2	3.5	n.s.	30.5	6.2	0.000	30.4	6.9	0.000	n.s.
$\gamma_{pel}$	GR	24.8	4.2	0.000	10.6	5.9	n.s.	-9.6	6.1	n.s.	0.000
	R	26.8	3.4	0.001	12.2	5.5	n.s.	-12.7	5.3	n.s.	0.000

## Supplement

Table S1: Amplitudes  $a_0$ ,  $a_1$ ,  $a_2$  and phases  $\varphi_1$ ,  $\varphi_2$  of the fit Fourier-terms  $y = a_0 + a_1 \sin(2\pi \cdot (t + \varphi_1)/100) + a_2 \sin(2 \cdot 2\pi \cdot (t + \varphi_2)/100)$ . GR, R: grounded running, aerial running;  $p \varphi_1$ ,  $\varphi_2$ : Significance with respect to uniform distribution (circular statistics)  $p_{GR\_R}$ : significance between grounded and aerial running (circular statistics). Bonferroni: 441 comparisons.

		$a_0$ [deg]		$a_1$ [deg]		$\varphi_1$ [%T]		$a_2$ [deg]		$\varphi_2$ [%T]		$p \varphi_2$	$r^2$	
		mean	SD	mean	SD	mean	SD	mean	SD	mean	SD		mean	SD
$\theta_{hip}$	GR	113.58	9.55	13.43	2.30	83.4	2.5	6.10	1.19	40.4	4.7	0.000	0.99	0.01
	R	121.10	6.27	16.90	2.50	87.2	1.8	6.58	0.99	48.4	4.1	0.000	0.99	0.01
	$p_{GR\_R}$					0.020				0.002				
$\theta_{kne}$	GR	109.67	3.07	24.18	2.69	31.5	2.4	15.57	1.77	49.8	4.0	0.000	0.98	0.01
	R	109.11	0.67	24.29	1.90	33.2	1.7	16.60	1.46	54.6	3.0	0.000	0.99	0.01
	$p_{GR\_R}$					n.s.				0.020				
$\theta_{ank}$	GR	117.55	3.58	13.28	4.95	69.0	5.5	17.45	4.44	42.5	6.7	0.000	0.85	0.05
	R	117.39	3.29	13.08	4.35	71.7	3.9	17.48	3.22	47.8	3.7	0.000	0.92	0.02
	$p_{GR\_R}$					n.s.				n.s.				
$\alpha_{hip}$	GR	-10.05	3.55	3.48	2.10	24.5	7.7	1.95	0.54	74.1	8.1	0.000	0.92	0.07
	R	-8.85	4.84	2.22	1.68	21.7	12.4	1.98	0.48	78.7	5.9	0.000	0.88	0.08
	$p_{GR\_R}$					n.s.				n.s.				
$\beta_{hip}$	GR	-73.91	15.62	13.55	2.02	84.6	2.5	3.82	1.28	34.9	5.9	0.000	0.99	0.01
	R	-64.79	10.32	16.37	3.40	87.8	1.4	4.73	1.22	41.9	5.5	0.000	0.98	0.05
	$p_{GR\_R}$					n.s.				n.s.				
$\gamma_{hip}$	GR	-5.17	5.06	6.34	3.70	68.7	12.3	4.14	1.51	20.2	9.2	0.000	0.88	0.10
	R	-8.09	4.77	6.57	1.32	79.3	7.8	4.21	1.11	27.0	5.5	0.000	0.93	0.09
	$p_{GR\_R}$					n.s.				n.s.				
$\alpha_{ank}$	GR	13.10	3.97	8.85	5.00	70.3	10.3	3.10	1.56	76.3	11.0	0.000	0.78	0.18
	R	10.89	3.26	11.84	3.89	66.6	9.5	4.43	0.98	83.9	10.3	0.001	0.92	0.10
	$p_{GR\_R}$					n.s.				n.s.				
$\beta_{ank}$	GR	-59.99	4.39	16.37	5.96	69.5	6.1	18.56	5.65	41.8	7.6	0.000	0.85	0.05
	R	-60.84	3.68	15.31	5.27	71.2	4.3	17.39	4.15	47.5	3.8	0.000	0.92	0.02
	$p_{GR\_R}$					n.s.				n.s.				
$\gamma_{ank}$	GR	5.64	2.56	8.46	2.47	71.4	8.7	4.70	2.09	37.0	17.3	0.005	0.77	0.14
	R	3.38	2.32	7.09	1.65	67.9	9.5	2.76	1.75	2.0	16.8	n.s.	0.88	0.10
	$p_{GR\_R}$					n.s.				n.s.				
$\alpha_{lum}$	GR	0.00	4.95	9.58	2.99	77.7	4.2	0.71	0.36	38.4	21.8	n.s.	0.98	0.01
	R	-0.09	2.27	7.82	2.62	80.1	3.6	1.14	0.67	52.4	21.1	n.s.	0.96	0.10
	$p_{GR\_R}$					n.s.				n.s.				
$\beta_{lum}$	GR	-0.75	3.22	2.44	1.13	53.0	17.1	3.88	1.14	46.4	4.4	0.000	0.90	0.06
	R	2.16	3.40	2.67	1.54	78.3	19.4	4.96	1.27	57.4	3.7	0.000	0.91	0.06
	$p_{GR\_R}$					n.s.				0.002				
$\gamma_{lum}$	GR	-0.02	3.24	8.83	2.23	31.3	3.7	1.00	0.58	19.6	20.1	n.s.	0.89	0.04
	R	-0.50	4.58	11.89	2.56	32.0	2.6	2.01	1.52	72.3	21.0	n.s.	0.91	0.03
	$p_{GR\_R}$					n.s.				n.s.				
$\alpha_{tho}$	GR	-0.07	5.26	4.28	1.93	26.8	11.6	0.57	0.35	33.7	21.5	n.s.	0.94	0.09
	R	-0.20	2.91	2.97	1.96	26.9	7.8	0.89	0.39	8.5	20.6	n.s.	0.93	0.03
	$p_{GR\_R}$					n.s.				n.s.				
$\beta_{tho}$	GR	36.61	9.88	2.03	1.02	2.9	14.7	2.93	0.83	89.3	5.1	0.000	0.87	0.05
	R	29.12	5.87	1.85	1.01	7.4	15.8	3.98	1.08	98.9	3.0	0.000	0.89	0.08
	$p_{GR\_R}$					n.s.				0.020				
$\gamma_{tho}$	GR	-0.10	6.50	6.26	1.88	5.4	6.5	1.08	0.75	71.7	20.5	n.s.	0.92	0.09
	R	0.77	4.55	6.64	1.78	1.8	6.4	1.89	1.80	7.5	22.5	n.s.	0.91	0.05
	$p_{GR\_R}$					n.s.				n.s.				
$\alpha_{pel}$	GR	-0.05	3.03	5.87	1.65	78.5	3.9	0.46	0.25	88.3	22.1	n.s.	0.98	0.02
	R	-0.27	3.65	4.89	1.08	81.0	3.4	0.38	0.28	12.2	18.2	n.s.	0.95	0.12
	$p_{GR\_R}$					n.s.				n.s.				
$\beta_{pel}$	GR	35.79	11.66	1.12	0.67	73.9	22.1	2.24	0.50	58.3	4.4	0.000	0.89	0.08
	R	31.39	6.03	1.86	1.17	96.6	13.1	2.72	0.49	70.3	3.8	0.000	0.86	0.09
	$p_{GR\_R}$					n.s.				0.002				
$\gamma_{pel}$	GR	-0.11	5.55	10.11	2.08	22.0	2.7	0.79	0.56	21.7	21.5	n.s.	0.95	0.03
	R	0.21	5.20	11.52	1.32	23.5	2.6	1.08	0.66	79.1	21.2	n.s.	0.97	0.02
	$p_{GR\_R}$					n.s.				n.s.				

Fig. S1

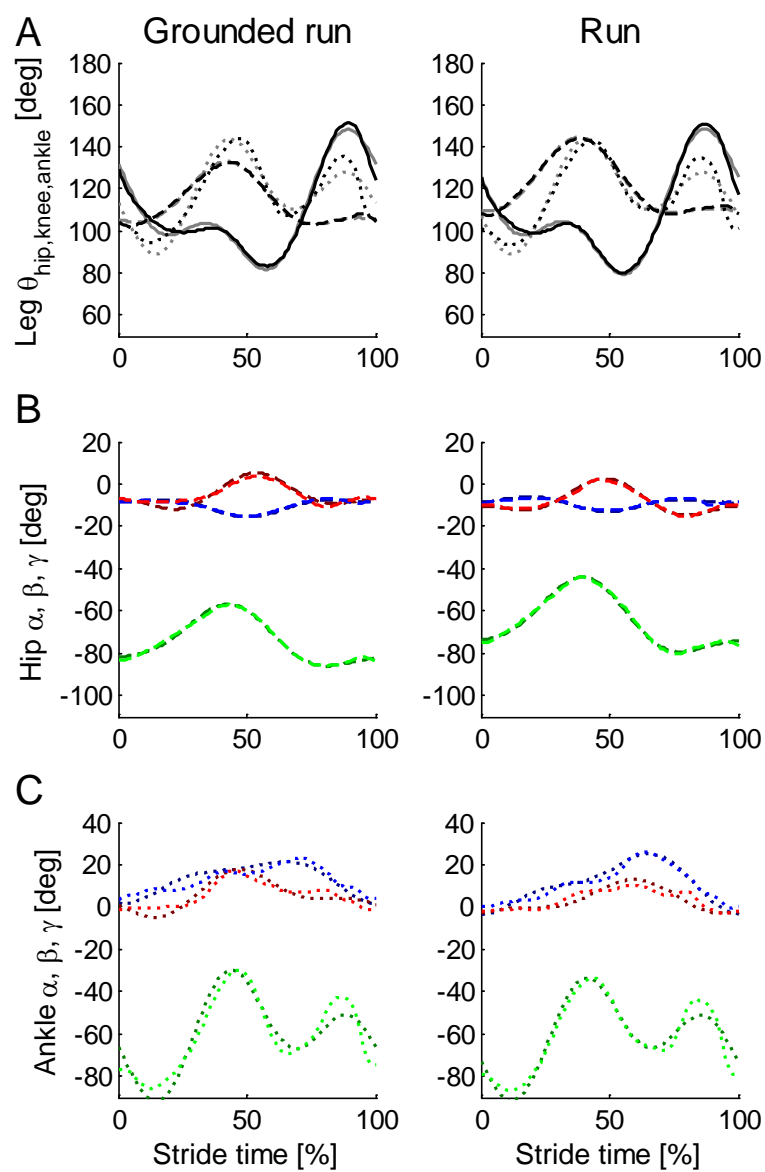


Fig. S1: Truncated Fourier-fit (dark tracings; comp. Table S1) to measurements obtained for measured leg angles (light colors; angle definitions, colors and line types see Fig. 3).

Fig. S2

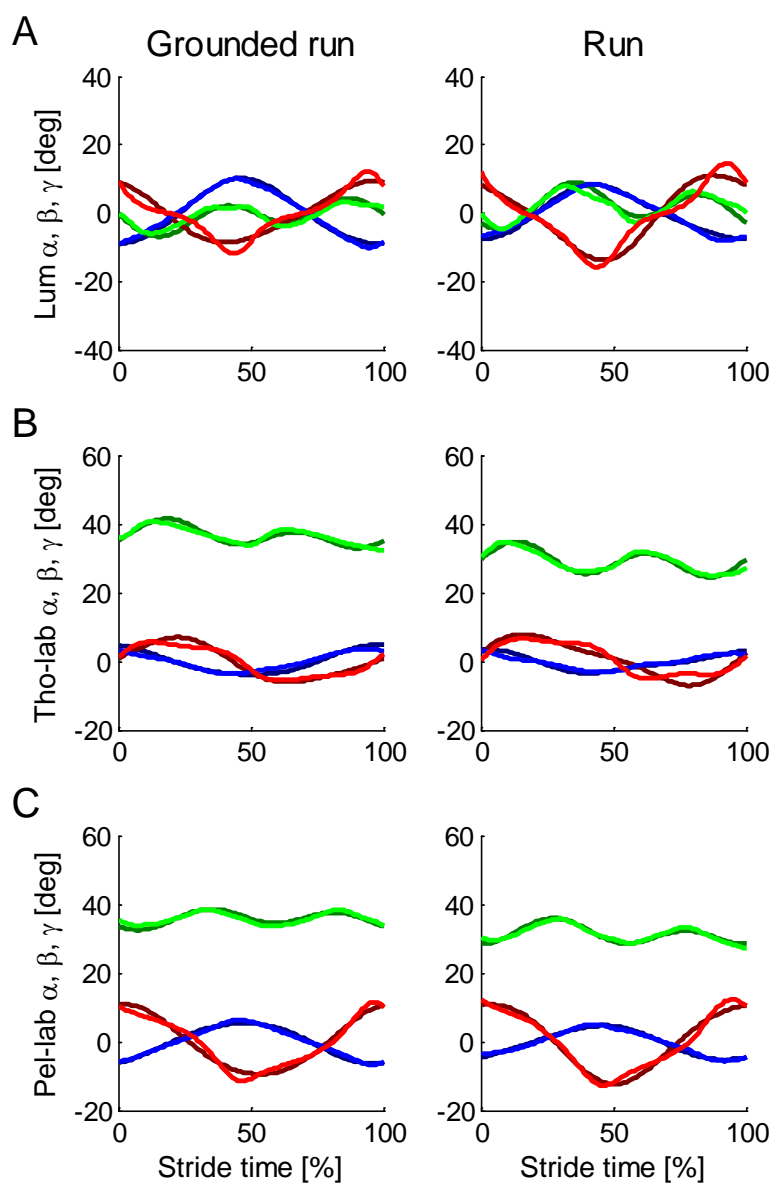


Fig. S2: Truncated Fourier-fit (dark tracings; comp. Table S1) to measurements obtained for measured trunk angles (light colors; for angle definitions, colors and line types see Fig. 6).